The role of groundwater in the Amazon water cycle: 1. Influence on seasonal streamflow, flooding and wetlands

Gonzalo Miguez-Macho[1] and Ying Fan[2]

Received 30 January 2012; revised 8 May 2012; accepted 10 May 2012; published 14 August 2012.

[1] Observational studies across the Amazon report a common occurrence of shallow water table in lowland valleys and groundwater-surface water exchange from small headwater catchments to large floodplains. In this study, we assess groundwater's role in the Amazon surface water dynamics using a continental-scale coupled groundwater-surface water model (LEAF-Hydro-Flood) forced by ERA-Interim reanalysis, at 2 km and 4 min resolution over 11 years (2000–2010). The simulation is validated with observed streamflow, water table depth and flooding extent. A parallel simulation without groundwater is conducted to isolate its effect. Our findings support the following hypotheses. First, in the headwater catchments, groundwater dominates streamflow; the observed variations in its dominance across the Amazon can be explained by the varying water table depth. Second, over large floodplains, there are two-way exchanges between floodwater and groundwater as infiltration in the wet season and seepage in the dry season, and the direction and magnitude are controlled by the water table depth. Third, the Amazon harbors large areas of wetlands that are rarely under floodwater and difficult to observe by remote sensing, but are maintained by a persistently shallow water table. Fourth, due to its delayed and muted response to rainfall, groundwater seepage persists in the dry season, buffering surface waters through seasonal droughts. Our simulations shed new lights on the spatial-temporal structures of the hidden subsurface hydrologic pathways across the Amazon and suggest possible mechanisms whereby groundwater actively participates in the Amazon water-carbon cycle such as CO_2 outgassing from groundwater seeps and CH_4 emission from groundwater-supported wetlands.

Citation: Miguez-Macho, G., and Y. Fan (2012), The role of groundwater in the Amazon water cycle: 1. Influence on seasonal streamflow, flooding and wetlands, *J. Geophys. Res.*, *117*, D15113, doi:10.1029/2012JD017539.

1. Introduction

[2] Groundwater and surface water are closely linked in most hydrologic settings [*Winter et al.*, 1998]; the groundwater reservoir receives surplus in wet periods and sustains rivers and wetlands in dry periods; a shallow water table impedes land drainage and affects soil moisture and evapotranspiration (ET). The potential influence of groundwater on ET has motivated recent efforts to include groundwater in climate and ecosystem modeling studies (e.g., *York et al.* [2002]; *Gutowski et al.* [2002]; *Liang et al.* [2003]; *Maxwell and Miller* [2005]; *Yeh and Eltahir* [2005]; *Kollet and Maxwell* [2006]; *Bierkens and van den Hurk* [2007]; *Niu et al.* [2007]; *Gulden et al.* [2007]; *Fan et al.* [2007]; *Miguez-Macho et al.* [2007, 2008]; *Lo et al.* [2008]; *Maxwell and Kollet* [2008]; *Anyah et al.* [2008]; *Yuan et al.* [2008]; *Zeng and Decker* [2009]; *Jiang et al.* [2009]; *Lo et al.* [2010]; *Fan and Miguez-Macho* [2010, 2011]; *Ferguson and Maxwell* [2010]; *Rihani et al.* [2010]; *Lo and Famiglietti* [2010, 2011]; *Choi and Liang* [2010]; *Niu et al.* [2011]; *Yang et al.* [2011]; *Yuan and Liang* [2011]; *Lam et al.* [2011]; among others). Emerged from these studies is that groundwater may function as a spatial organizer of soil moisture by maintaining wet valley floors via lateral groundwater flow, and a temporal buffer for soil moisture and river discharge by its delayed and small-amplitude response to weather and climate fluctuations.

[3] In this study, we investigate groundwater's role in the seasonal water cycle of the Amazon, the largest river system and home to the most extensive tropical-forest on the planet. The seasonal migration of the Inter-Tropical Convergence Zone (ITCZ) over the Amazon leads to pronounced seasonality in rainfall and distinct seasonal swings in soil moisture, river flow and floodplain inundation. Because groundwater is the slowest and most stable component of the

[1]Nonlinear Physics Group, Faculty of Physics 15782, Universidade de Santiago de Compostela, Galicia, Spain.
[2]Department of Earth and Planetary Sciences, Rutgers, State University of New Jersey, New Brunswick, New Jersey, USA.

Corresponding author: Y. Fan, Department of Earth and Planetary Sciences, Rutgers, State University of New Jersey, New Brunswick, NJ 08854, USA. (yingfan@rci.rutgers.edu)

©2012. American Geophysical Union. All Rights Reserved.
0148-0227/12/2012JD017539

land hydrologic stores, we hypothesize that it modulates the magnitude and timing of seasonal changes in Amazon surface water stores. We examine the seasonality in groundwater and its influence on the seasonality of soil moisture, ET, river flow and flooding. In this first of a two-part series, we focus on groundwater exchange with rivers, floodplains and wetlands. In the companion paper [*Miguez-Macho and Fan*, 2012] we examine groundwater's influence on soil moisture and ET flux. They are in this order because model validation, using the more abundant surface water observations, should precede discussions of modeled soil moisture and ET, which are scantly observed. Our tool is a continental-scale, high-resolution (~2 km) land model with a prognostic groundwater reservoir and river-floodplain routing. The model has been applied to studying the co-evolution of groundwater, river flow, soil moisture, and land-atmosphere interaction over N. America [*Miguez-Macho et al.*, 2007; *Anyah et al.*, 2008].

[4] There exists a substantial body of literature on the Amazon surface water dynamics. Most informative are field observations of water, sediment and biogeochemical fluxes in the complex river-floodplain-lake system. The work of *Richey et al.* [1989a, 1989b] gave the first assessment of the importance of Amazon floodplains in regulating seasonal discharge; they estimated that ~30% of Amazon discharge has once passed the floodplains. *Meade et al.* [1991] illustrated the importance of backwater on river stage and discharge in the Amazon main channel and lower tributaries; because of the large basin size, the out-of-phase northern-southern wet season, and the low gradient, upstream discharge is inhibited by rising waters in the lower reach, giving hysteretic stage-discharge relations. Other important findings came from detailed coring and mapping of floodplain sediments by *Räsänen et al.* [1990, 1992], *Kalliola et al.* [1991, 1992], *Mertes et al.* [1996], *Mertes* [1997], *Dunne et al.* [1998] and *Aalto et al.* [2003], revealing active subsidence and sedimentation in the Andean foreland basins and strong geologic controls on channel-floodplain morphology. The remoteness of the Amazon makes remote sensing a unique tool for studying flooding dynamics; satellite and shuttle images reveal meter-scale complexity in river-floodplain exchange and the strong topographic control at rising water and hydraulic control at falling stage in the annual flood cycle [*Alsdorf et al.*, 2007; *Hess et al.*, 2003; *Melack et al.*, 2004].

[5] Of particular relevance to this work, concerning groundwater, are water budget studies at two distinct scales. The first focused on small, headwater catchments where the hilltops are well drained followed by groundwater flow toward the valleys. A common finding across the Amazon is that surface runoff is rare and deep soil infiltration and subsequent down-valley groundwater convergence accounts for >90% of river discharge as base flow [*Lesack*, 1993; *Leopoldo et al.*, 1995; *Grogan and Galvão*, 2006; *Hodnett et al.*, 1997a, 1997b; *Cuartas*, 2008; *Neu et al.*, 2011]. The slow groundwater convergence leads to a persistently shallow water table in the valleys and a delay in water table rise after the onset of the rainy season [*Hodnett et al.*, 1997a, 1997b; *Johnson et al.*, 2006a; *Grogan and Galvão* 2006; *Cuartas*, 2008; *Vourlitis et al.*, 2008; *Tomasella et al.*, 2008]. The study of *Tomasella et al.* [2008] further shows that groundwater memory can be carried beyond the next season as to influence the water balance in the coming years.

[6] The second group of studies focused on groundwater's presence in the lower floodplains that are dominated by surface water dynamics. Water budget, turbidity, and chemical tracer analyses of *Forsberg et al.* [1988], *Mertes* [1997], *Hamilton et al.* [2007], and *Bourrel et al.* [2009] suggest two distinct water sources on the floodplain, one from overbank flooding of river water of external origin (white water with high sediment-nutrient load, from the Andes), and the other from small tributaries fed by groundwater seepage of local origin (black or clear water, low in sediment-nutrient). Water budget studies in central floodplain lakes also document groundwater seeps [*Lesack*, 1995; *Lesack and Melack*, 1995; *Cullmann et al.*, 2006; *Bonnet et al.*, 2008]. Seepage is also observed in the seasonally flooded forest-savanna in Bananal Island in the southeastern Amazon [*Borma et al.*, 2009] where steady groundwater drainage from higher grounds maintains the water level in floodplain lakes in the dry season. Thus it appears that even in the floodplains of the Amazon that are overwhelmed by surface water dynamics, groundwater can be present, which can have distinct geochemical contributions due to its subsurface flow paths.

[7] The extensive observational insights gained from the above field studies (and many more not mentioned here), and the careful syntheses by the above investigators, have written a rich narrative of the Amazon River system from the headwaters to its extensive floodplains. These insights are of fundamental importance to modeling studies such as ours, because they uncover key physical processes that must be considered by process-based models.

[8] Modeling studies at the Amazon basin scales are represented by the recent work of *Costa and Foley* [1997], *Foley et al.* [2002], *Chapelon et al.* [2002], *Coe et al.* [2002, 2008], *Wilson et al.* [2007], *Beighley et al.* [2009], *Decharme et al.* [2008, 2010], *Alkama et al.* [2010], and *Yamazaki et al.* [2011], among others. These models in general include two components, the first calculating land-surface fluxes (ET, surface runoff and deep soil drainage) involving soil and vegetation stores, and the second routing surface runoff and soil drainage through the river-floodplain system to the ocean. These studies demonstrated the feasibility of modeling such a large and complex system, and revealed model sensitivities to land-surface parameters particularly floodplain and channel morphology. Of unique importance to our work is *Coe et al.* [2008] which gave empirical relationships between river hydraulic geometry at a given point in the network and the drainage area above the point using observations from the Amazon, whereas commonly used relationships are derived from data on N. American rivers. Another study of unique importance is *Yamazaki et al.* [2011], which simulated backwater effects globally by explicitly solving the diffusive wave equation, which had not been achieved before due to numerical instabilities at large time steps needed for global models. These two studies exemplify recent advances in realistically representing Amazon surface water dynamics at the whole basin scale.

[9] Absent from the above modeling studies is a prognostic groundwater reservoir below the land surface that is

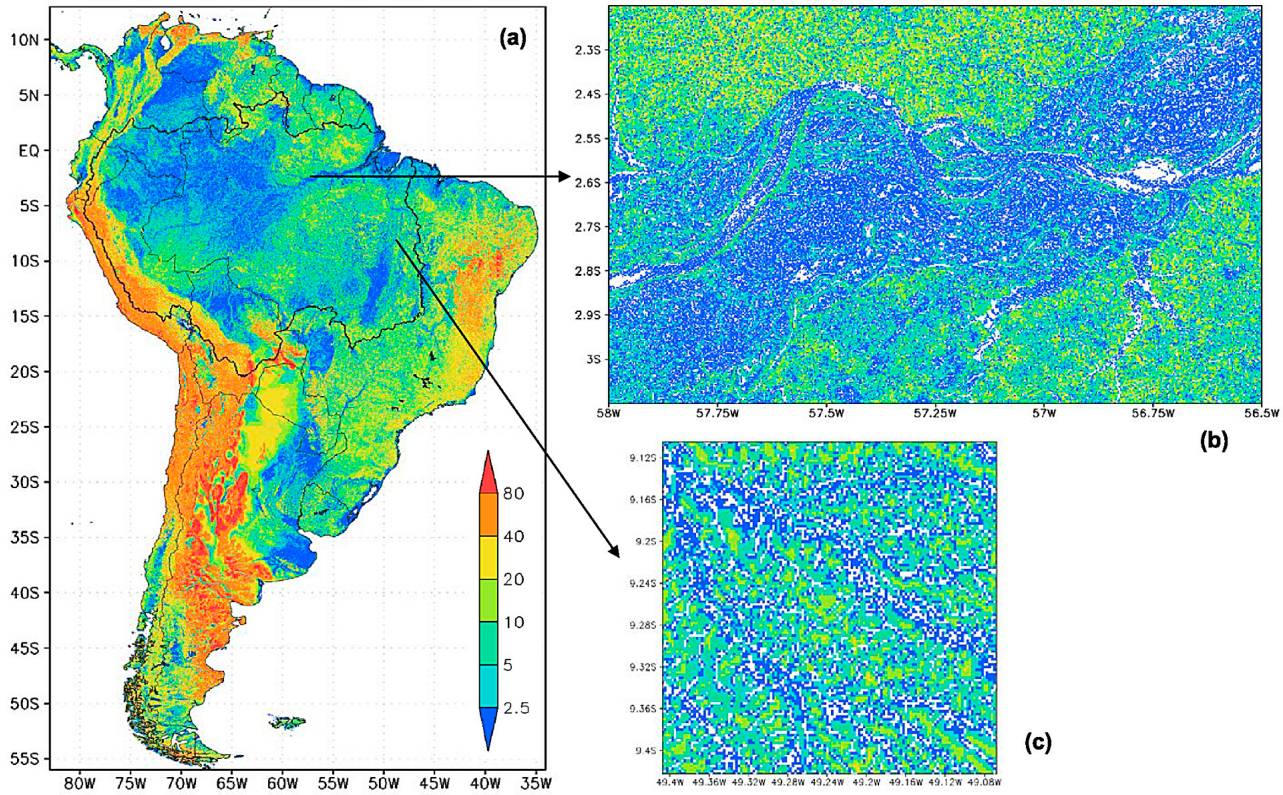

Figure 1. (a) Simulated climatologic mean water table depth (in meter below land surface, at 9″ grids) over South America, (b) details over floodplain, and (c) details over the seasonally dry eastern Brazil (white cells mark groundwater emergence at the land surface).

dynamically coupled to the surface stores. As referenced above, rivers and floodplains receive groundwater seeps, but they also lose water by infiltration into valley and floodplain sediments; this two-way exchange is governed by their relative water surface elevation and contact area. Some of the current models include a subsurface store with controlled release to streams such as a calibrated time delay, but it remains a passive receiver of upland drainage without affecting the latter, and with one-way release to the rivers without feedbacks to the groundwater. This lack of an interactive groundwater in current models is related to the fact that the importance of groundwater at the Amazon basin-scale is largely unknown. Although field studies have documented the dominant role of groundwater in upland drainage and groundwater-floodplain exchange in lowland swamps, its basin-wide significance and its time-scale interactions with surface water dynamics are not yet quantified across the Amazon. The objective of this study is to assess the basin-wide significance of groundwater, through modeling the two-way mechanistic links between groundwater and surface waters across the Amazon. Our goal is to elucidate groundwater flow paths and the time-scale interactions between the slow and stable groundwater and the fast changing surface waters from headwater catchments to large floodplains. We start with the following question: how close is the groundwater to the land surface? Is there sufficient evidence across the Amazon that it is close enough to warrant further inquiries?

[10] Figure 1 gives the climatologic equilibrium water table depth (WTD) in S. America from a simple two-dimensional groundwater model at 9 arc-second (~270 m) grids, validated with 34,351 well observations [*Fan and Miguez-Macho*, 2010]. Its purpose is to give a first-order view of groundwater proximity to the land surface. The water table recharge (R) is annual precipitation (P) subtracting ET and surface runoff (SR): $R = P$-ET-SR. We obtained ET and SR from four global land models: HTESSEL, CLM, MOSAIC, and NOAH forced by observed or reanalysis rainfall. The HTESSEL is the land model of ECMWF global climate model [*Balsamo et al.*, 2009] whose reanalysis is used to force the simulations later in this study, and CLM, MOSAIC, and NOAH are participants in NASA's Global Land Data Assimilation System (GLDAS) [*Rodell et al.*, 2004]. We found that the simulated WTD is relatively insensitive to differences in recharge due to negative feedbacks between recharge and water table height [*de Vries*, 1994, 1995; *Eltahir and Yeh*, 1999; *Marani et al.* 2001]. The simulation in Figure 1 is forced by HTESSEL. Sea level along the coast is the hydraulic head boundary condition. We note that the WTD in Figure 1 is obtained from model recharge estimate without groundwater feedbacks; it is only a first guess used here to initialize fully coupled simulations discussed later, and to infer broad patterns in WTD qualitatively. The latter is why Figure 1 is introduced here.

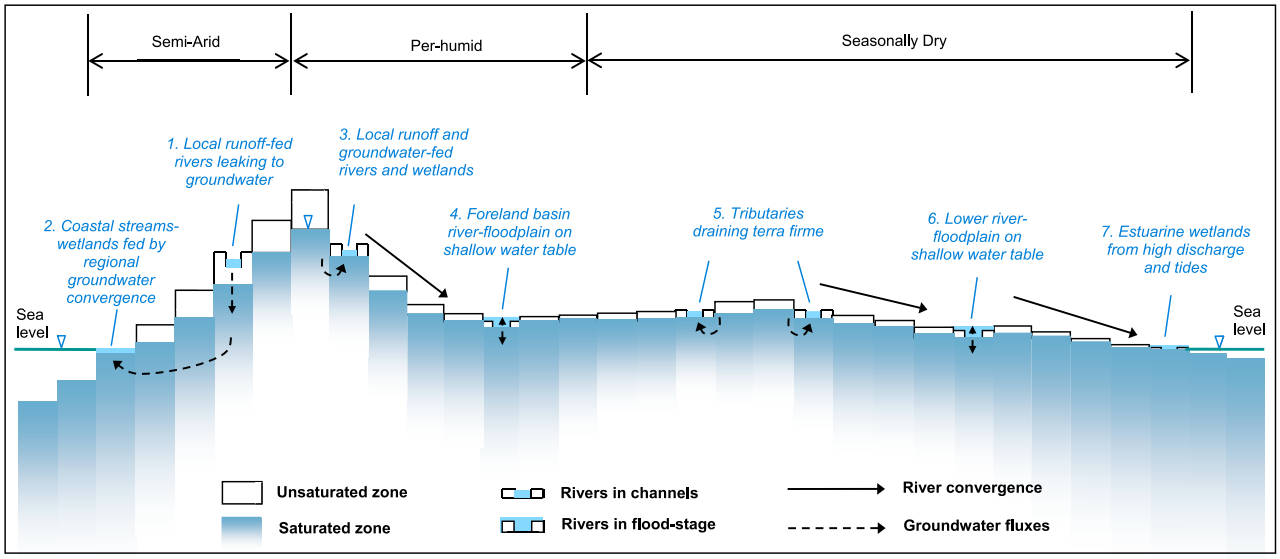

Figure 2. A simple conceptualization of potential groundwater influence on surface water features along the main stem of Amazon.

[11] It suggests that the water table can be shallow under large areas. Examples are the humid lowland basins of the Orinoco (Colombia and Venezuela, ~6°N) and the Andean foreland basins (eastern Peru and western Brazil, ~5°S); the seasonally dry Beni and Mamore Basins (Bolivia, ~14°S), the Bananal Island (central Brazil, ~12°S) and the Pantanal (southern Brazil, ~17°S); and the still drier Parana valley and Pampas Plains (Argentina, ~25–38°S), which are lowlands receiving regional groundwater convergence despite local climate. At local scales, Figure 1b reveals a band of shallow water table under the Amazon floodplain (white cells indicate groundwater seeps), and Figure 1c suggests a deep water Table (10–40 m) under uplands but shallow in the valleys; it is well known that the shallow groundwater in the valleys here supports lush gallery forests along river corridors in the otherwise dry Cerrado landscape [*Prance*, 1987; *Clapperton*, 1993].

[12] Available field observations across the Amazon also suggest an ubiquitously shallow water table in the foreland basins and all river valleys, and a varied depth of 5–40 m under uplands (*Brazilian Geological Survey* as compiled in *Fan and Miguez-Macho* [2010]; *Bongers et al.* [1985]; *Poels* [1987]; *Lesack* [1995]; *Coomes and Grubb* [1996]; *Hodnett et al.* [1997a, 1997b]; *McClain et al.* [1997]; *Selhorst et al.* [2003]; *Grogan and Galvão* [2006]; *Jirka et al.* [2007]; *Tomasella et al.* [2008]; *Cuartas* [2008]; *Vourlitis et al.* [2008]; *Borma et al.* [2009]; *Lähteenoja and Page* [2011]; and *Neu et al.* [2011]). If indeed the water table is near the land surface and in direct physical contact with surface water features, there is a need to conceptualize the Amazon surface water hydrology taking into account the potential influence of the groundwater.

[13] Figure 2 is such an attempt. It illustrates potential groundwater influences on local and regional surface water features, drawn in a schematic west-east transect from coastal Peru to Amazon estuary, guided by the generalized section of *Dunne and Mertes* [2007], and illustrated as grid cells to place the discussion in a modeling context. On the western slope of the Andes, the dry climate supports small streams fed by local runoff in valley alluvium, but the streams lose their waters to the regional aquifer below (surface water feature 1) through which they move down the regional gradient and emerge in the lower valleys to feed streams and wetlands (feature 2). On the eastern slope of the Andes, the per-humid climate and steep terrain maintains perennial streams from local runoff (feature 3). Numerous such rivers join and descend the eastern slope, converging in the foreland basins (the Andean trough), inundating and filling them with sediments; they are termed white-water rivers due to large suspended sediment loads; here the river courses are highly dynamic and often elevated, leaving behind a complex package of floodplain sediments and interconnected channels and lakes at high waters (feature 4). As the middle Amazon (Solimoes) traverses the continent eastward, it collects large tributaries (black and clear water, low nutrient and sediment) draining forests and savannas (feature 5) on both sides of the Equator, with extensive flooding in the lower valleys. As the Amazon cuts through the cratonic shields (Guyana Highlands to the north and Brazilian Highlands to the south) and collects more tributaries, it floods the bedrock-restricted floodplains (feature 6). As the Amazon nears the sea, vast wetlands form, influenced by both the large volume of Amazon discharge and the tides (feature 7).

[14] Based on our earlier synthesis of field observations, we hypothesize that several of these surface water features may interact with the groundwater through the following mechanisms. First, in the headwater catchments across the Amazon, groundwater is the dominant source of streamflow (feature 3 and 5, Figure 2), but the magnitude varies from one place to another because of the varying water table depth; a shallow water table inhibits deep infiltration and hence

groundwater contribution to streamflow, and it enhances surface saturation and hence saturation-excess (or Dunne) runoff. Second, in the lower floodplains across the Amazon, there are two-way exchanges between the floodwater and the groundwater (feature 4 and 6); in the wet season, rainfall and the rising-expanding floodwater infiltrate into the floodplain sediments, but the amount of infiltration is limited by the shallow water table; in the dry season, the flow reverses, and groundwater seeps out to feed floodplain lakes and wetlands. Third, groundwater supports wetlands rarely under floodwater but characterized with a persistently shallow water table, creating water-logged conditions defining wetlands. Since non-flooded wetlands are difficult to observe by remote sensing, their potential contribution to the Amazon carbon output through methane emission has been difficult to assess. Fourth, the longer time scales of groundwater regulate river flow and surface flooding dynamics; because of its delayed and muted response to rainfall, groundwater seeps may peak and persist in the dry season. The above mechanisms have been observed in isolated parts of the Amazon, and in this study, we provide a model synthesis and assessment of basin-scale significance of these mechanisms; the true test of the above hypotheses must come from large-scale field instrumentations.

[15] Groundwater and surface water is a continuum and can exchange at multiple times along their flow paths from the uplands to the ocean [*Winter et al.*, 1998]; there are an infinite number of flow paths in a vast fluvial system like the Amazon; and the paths initiate at different times as dictated by land-surface water budget in response to the atmosphere at a range of time scales. A modeling framework, tracking both surface and subsurface flow paths and exchanges, and informed by observations, can provide a laboratory to test the hypotheses posed above. A detailed and systematic view of groundwater flow pathways and residence times, from headwater catchments to lower floodplains, is useful for understanding carbon and nutrient export pathways out of the Amazon [*Richey et al.*, 2009, 2011] which is in turn needed for understanding the Amazon ecosystem's role in the global carbon budget. The goal of this study is to elucidate the groundwater flow paths and their exchanges with the surface drainage of the Amazon basin. We will use a coupled groundwater-surface water model, forced by reanalysis atmosphere, run at fine resolutions ($\sim$2 km) over the whole basin, at small time steps (4 min) over 11 years (2000–2010), and validated with surface and groundwater observations, to examine daily, seasonal, and inter-annual dynamics at catchment to continent scales. The model is described in section 2, forcing, parameters and simulations in section 3, validations in section 4, results and analyses in section 5, and a summary in section 6 with a discussion of potential implications to Amazon carbon cycle.

2. Model Description

[16] The model we use is called LEAF-Hydro-Flood. LEAF (Land-Ecosystem-Atmosphere Feedback) is the land-surface component of RAMS (Regional Atmosphere Modeling System), a regional climate model developed at Colorado State University and widely applied to climate research. Detailed descriptions of LEAF physics are given in *Walko et al.* [2000]. It includes prognostic water and thermal energy in multiple layers of soil and snow, a surface store (ponding water), a vegetation canopy, and a canopy air, and includes turbulent and radiative exchanges between these components and with the atmosphere. Each land grid cell can be subdivided to multiple patches, each with distinct topography, soil and vegetation characteristics. Within each patch, vertical soil water flux is calculated using the Richards equation. A TOPMODEL [*Beven and Kirkby*, 1979] framework is used to allow lateral soil water movement among the patches to a depression, but it does not include a river network to route the drainage out of the grid. Further descriptions on soil water fluxes can be found in the companion paper. Note that in our study we do not subdivide a grid into patches, and have completely replaced the TOPMODEL component with the processes described next.

[17] Several major changes were made to LEAF through our earlier work on N. America [*Miguez-Macho et al.*, 2007], resulting in LEAF-Hydro. The changes were (1) extending the soil column to the dynamic water table below, the latter acting as saturation boundary condition and affecting soil water flux above, (2) allowing the water table, once recharged by rain events, to relax through discharge into rivers within a grid cell and lateral groundwater flow among adjacent cells, leading to divergence from high grounds and convergence to low valleys at multiple scales, (3) allowing two-way exchange between groundwater and rivers depending on hydraulic gradient, representing both loosing (leaking to groundwater) and gaining (receiving groundwater) streams, (4) routing river discharge, fed by surface runoff and groundwater convergence, to the ocean through the channel network using the kinematic wave method, and (5) setting the sea level as the groundwater head boundary condition, hence allowing sea level to influence coastal drainage. In this study, we further introduce a new river-floodplain routing scheme that solves the full momentum equation of open channel flow, taking into account the backwater effect (the diffusion term) and the inertia of large water mass of deep flow (the acceleration terms) that are important in the Amazon. To differentiate from the earlier version, we will refer to the model here as LEAF-Hydro-Flood. Details of process coupling (1 to 5 above) are given in *Miguez-Macho et al.* [2007]. We briefly highlight the key elements below, with emphasis on the new flooding scheme.

2.1. Extending the Soil Column to the Water Table

[18] The standard (without groundwater) LEAF soil column configuration, with 11 layers extending to 2.5 m depth, is shown in the upper portion of Figure 3a (black; colors indicating changes we made). Downward gravity drainage (G) and bi-directional capillary flux (C) are obtained from solving the Richard's equation. Three more layers (each 0.5 m thick) were added to extend the numerically resolved depth to 4.0 m. If the water table is within 4.0 m (Figure 3a, Water Table 1), saturation boundary condition occurs at this depth, above which soil water flux is calculated as before. If the water table is below 4.0 m (Figure 3a, Water Table 2), a variable thickness layer (shaded) is added to extend the soil column to the water table. The flux across the water table (recharge R) is converted to water table rise or fall according to the saturation level above the water table.

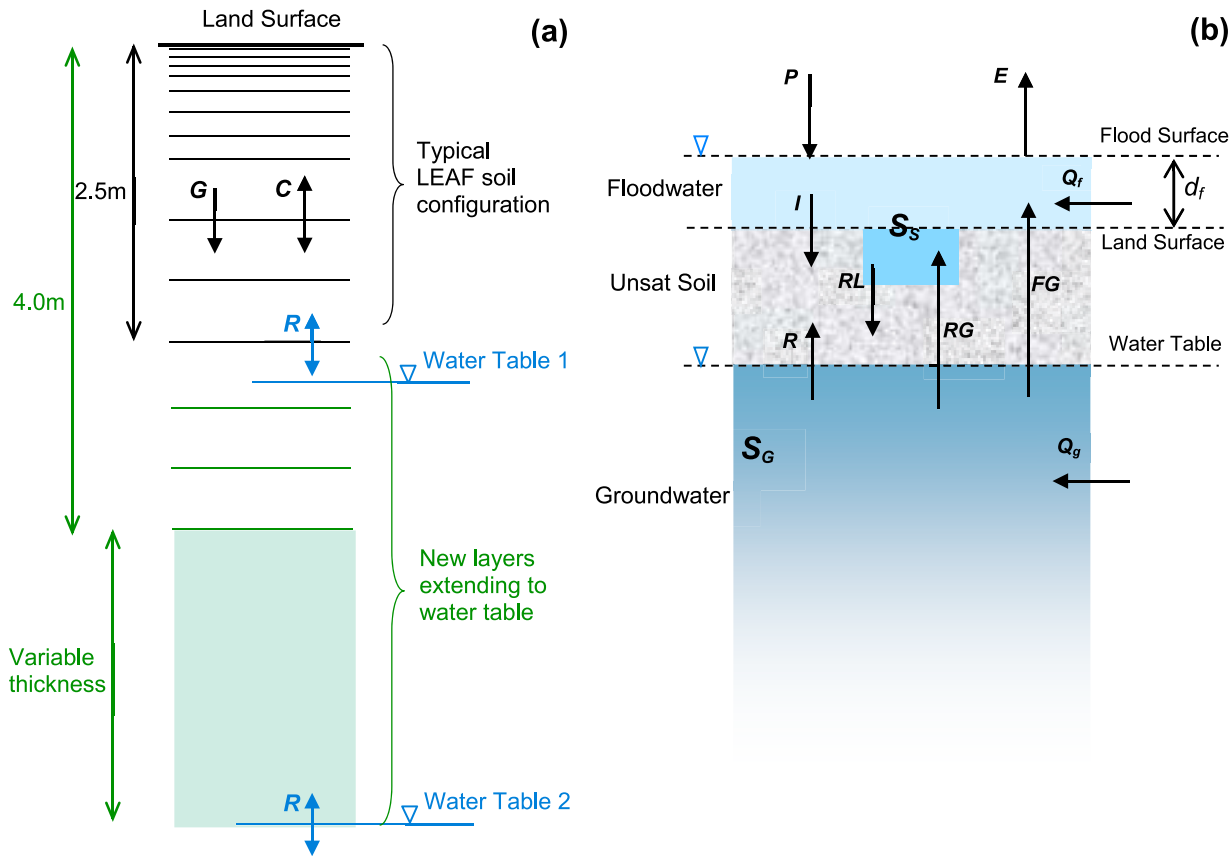

Figure 3. (a) Soil-groundwater coupling (color indicating changes made to LEAF), and (b) floodwater-river-groundwater coupling.

2.2. A Prognostic Groundwater Store and Two-Way Coupling With Surface Stores

[19] We explicitly track the mass balance in the groundwater store in each model cell

$$\frac{dS_G}{dt} = \Delta x \Delta y(-R - \mathrm{FG}) - \mathrm{RG} + \sum_{1}^{8} Q_g. \qquad (1)$$

[20] As shown in Figure 3b, S_G [L^3] is the groundwater store in a cell, R [L/T], standing for recharge, is the flux across the water table, FG [L/T] is groundwater-floodplain exchange, RG [L^3/T] is river-groundwater exchange, and Q_g [L^3/T] is the lateral groundwater flow from/to the eight neighboring cells calculated from Darcy's law. If the unsaturated soil zone (Figure 3b, gray layer) is absent, $R = 0$, and the groundwater directly interacts with the floodplain through FG [L/T] (otherwise FG = 0), which is groundwater seepage as a result of lateral groundwater convergence from neighboring cells. We note that a key groundwater process, lateral exchange with adjacent grid cells in addition to exchange with the surface waters within a cell, is accounted for here (last term in equation (1)), because regional groundwater flow can be

Table 1. Field Observations of Water Table Depth–Site Information and Data Source

		Longitude	Latitude	Observation Period	Source	Observed Mean WTD (m)		Modeled Mean WTD (m)	
						High Ground	Low Ground	High Ground	Low Ground
1	Acre	−67.6236	−10.0831	1999–2004	*Selhorst et al.* [2003]	−8.62	−5.90	−10.67	−5.98
2	Rancho Grande	−62.8667	−10.3333	2005	*Germer et al.* [2010]	−1.05		−1.83	
3	Jau National Park	−61.6375	−1.9125	2000–2001	*Do Nascimento et al.* [2008]	−1.38	−0.77	−2.10	−0.17
4	Asu	−60.2	−2.61	2002–2005	*Cuartas* [2008]	−17.32	−0.60	−15.17	−0.45
5	Juruena	−58.5	−10.5	2004–2005	*Jirka et al.* [2007]	−4.66	−1.20	−5.82	−1.77
6	Sinop	−55.325	−11.4125	2005–2006	*Vourlitis et al.* [2008]	−3.38		−6.46	
7	Redencao	−50.2227	−7.8333	1996–2001	*Grogan and Galvão* [2006]	−5.83	−1.32	−5.39	−1.41
8	Bananal Island	−50.1487	−9.8211	2003–2006	*Borma et al.* [2009]	−2.38	−0.87	−2.40	−1.50

important at a range of scales but particularly with small model grid cells and in deep aquifers such as found in large sedimentary settings [e.g., *Schaller and Fan*, 2009].

[21] The water in the river channel and floodplain within each cell makes up the river-floodplain store S_S [L^3]. At a given time step, if the river stage exceeds the bank height, the excess water is spread uniformly over the cell containing the channel, and the flood height is calculated with a surface elevation equal to that of the water in the river channel, now above bank height. The bank height, a critical parameter in determining flooding, is derived from topography and described in detail in section 3.1 (land-surface parameters). Floodplain water spreads to neighbor cells (Q_f) in eight directions, as determined by water surface elevation difference, or it returns to the channels as rivers recede. At the rising stage before the floodplain contains any water, flood water spreading is controlled by topography, as observed by *Alsdorf et al.* [2007]. The mass balance for the river-floodplain store (S_S) is

$$\frac{dS_S}{dt} = \mathrm{SR} + \mathrm{RG} + \Delta x \Delta y \mathrm{FG} + \sum_1^7 Q_i - Q_o - \Delta x \Delta y (I + E) + \sum_1^8 Q_f \quad (2)$$

where SR [L^3/T] is upland surface runoff from within the cell, Q_i [L^3/T] inflow from up to 7 upstream river cells, Q_o [L^3/T] river outflow to the downstream cell, E [L/T] evaporation from floodwater, I [L/T] infiltration loss of floodwater to the unsaturated soil below, and Q_f [L^3/T] floodwater movement among adjacent cells. The last three terms are only considered when the cell is flooded, or is one of the adjacent ones for the case of Q_f. The two water stores described by equations (1) and (2) are coupled through the two-way fluxes described below.

2.3. River-Floodplain Routing (Q_f, Q_i, Q_o)

[22] These three surface water fluxes are solved from the river and floodplain mass balance and momentum equation of open channel flow. The 1D momentum equation is [e.g., *Hunter et al.*, 2007]

$$\frac{\partial v}{\partial t} + v\frac{\partial v}{\partial x} + g\left(\frac{\partial d}{\partial x} + S_f - S_b\right) = 0 \quad (3)$$

where v is cross-section mean flow velocity [L/T], g gravitational acceleration [L/T^2], d flow depth [L], S_f friction slope and S_b river bed slope. The friction slope S_f was given by Manning as

$$S_f = \left(\frac{vn}{\mathrm{HR}^{2/3}}\right)^2 \quad (4)$$

where n is Manning's roughness coefficient, and HR [L] the hydraulic radius approximated by flow depth in a rectangular channel, an assumption valid in the Amazon [*Trigg et al.*, 2009].

[23] The first two terms in equation (3) represent the inertia force from local acceleration and advection, and the third term (with parentheses removed) the pressure force. Neglecting the first three terms gives the uniform flow or kinematic wave method, commonly applied for continental-scale river routing [e.g., *Decharme et al.*, 2010] and used in our earlier study in N. America [*Miguez-Macho et al.*, 2007]. It is the simplest approach where the velocity (v) can be obtained from equation (4) by letting $S_f = S_b$ in equation (3). Where the channel bed slope is steep and the flow is shallow, the method has been sufficient. However, it neglects the downstream boundary condition; flood movement is uninhibited by rising waters below. In the Amazon main channel and lower tributaries, backwater effect is widely noted [*Meade et al.*, 1991; *Trigg et al.*, 2009] and must be accounted for.

[24] To do so the third term in equation (3) (water depth differential) is needed. Summing the third and the last term (S_b) gives the water surface slope, which can be equated to the friction slope (S_f), and flow velocity (v) can be obtained by inverting equation (4). Since it leads to a partial differential equation in the form of the diffusion equation, it is referred to as the diffusion method (versus kinematic wave). However, explicit finite difference solutions to the diffusion equation are inherently unstable at fine grids [*Bates et al.*, 2010] unless the time step is reduced to seconds or solved implicitly [*Trigg et al.*, 2009], both computationally infeasible for our model domain and decadal simulations. Another option is to increase grid size; *Yamazaki et al.* [2011] solved the diffusion equation explicitly using grids of 25 km at time steps of 20 min globally. Increasing grid size is not ideal if we wish to retain the spatial details afforded by our 2 km-grid land model; the high resolution should also improve the simulation of floodplains strongly controlled by local topography.

[25] *Hunter et al.* [2007] and *Bates et al.* [2010] suggest that the lack of the inertia terms (first 2 terms in equation (3)) in deep flow problems (large mass) contributes to numerical instability, and *Bates et al.* [2010] proposed a quasi-explicit method that solves equation (3) with the acceleration term (first term) only. However, the method should be equally applicable to the full momentum equation with both inertia terms. Combining equations (3) and (4) and approximating HR (hydraulic radius) with d (flow depth) as commonly done, we obtain the following finite difference equation that is as implicit as possible while maintaining linearity in the unknown ($v_i^{t+\Delta t}$)

$$\frac{v_i^{t+\Delta t} - v_i^t}{\Delta t} + v_i^{t+\Delta t}\frac{v_{i+1}^t - v_i^t}{\Delta x} + g\frac{h_{i+1}^{t+\Delta t} - h_i^{t+\Delta t}}{\Delta x} + \frac{gn^2 v_i^t}{\left(d_i^{t+\Delta t}\right)^{4/3}} v_i^{t+\Delta t} = 0 \quad (5)$$

where d [L] is the water depth, and h [L] is the water surface elevation (the 3rd term above is the water surface slope). Equation (5) is linear in the unknown $v_i^{t+\Delta t}$ and can be solved explicitly. The water height at ($t + \Delta t$) is obtained from the mas continuity equation knowing the flow velocity from the previous time step. To achieve stability at 0.5 min time step (1/8 of Δt in our land model), we further adopted a second-order Runge-Kutta method [*Press et al.*, 1989] which uses a mid-point (0.25 min) trial time step so as to move the time derivative from backward difference (explicit formulation) closer to the center between two adjacent time steps. A similar method is used by *Yamazaki et al.* [2011]. In solving for the movement of floodwater across the floodplain to the eight neighboring cells, the inertial terms are neglected because the flow is much shallower than in river channels and the solution of the diffusion equation is more stable.

2.4. Evaporation From Floodwater Surface (*E*)

[26] Floodwater is incorporated into the surface water store already present in the standard LEAF for the purpose of calculating floodwater surface evaporation. Without flooding, the surface water store in standard LEAF did not reach significant depths, and evaporation was calculated assuming a uniform temperature for the whole depth, derived from thermal energy balance in the surface water store. However, with flooding, surface water can be several meters deep, and a homogeneous temperature is no longer valid, particularly for estimating surface evaporation. Hence we adopted a similar approach as in the lake model of the Community Land Model (CLM [*Oleson et al.*, 2010]) when the flooding depth is >5 cm. The surface water is represented as a two-layer system, with a skin layer interacting with the atmosphere above and a thick bottom layer below, the latter interacting with the soil below through energy balance in both stores and heat exchanges. Energy balance in the skin layer is used to obtain the skin temperature needed to calculate sensible and latent heat fluxes using the standard resistance formula already in LEAF.

2.5. River-Groundwater Exchange (RG)

[27] River-groundwater exchange occurs in two modes. The first is when the water table is above the river elevation and groundwater flows into the river (gaining stream). The second is when the water table is below the river elevation and groundwater receives leakage from the river (losing stream). The flux is calculated with Darcy's law following the widely used groundwater model MODFLOW developed by the U.S. Geological Survey [*Harbaugh et al.*, 2000]

$$\mathrm{RG} = \mathrm{RC} \cdot \left(h_g - h_r\right), \mathrm{RC} = \left(K_{rb}/b_{rb}\right)(\mathrm{WL}) \tag{6}$$

where h_g is the water table head in the cell, h_r river elevation, and RC [L^2/T] river hydraulic conductance. The latter measures the river-groundwater hydraulic connection and depends on river bed permeability K_{rb}[L/T], thickness of river bed sediment b_{rb} [L], river width W times length L in the cell (river-groundwater contact area). Lacking river bed information, we parameterize RC to reflect the essence of process coupling.

[28] It is well known that the river-groundwater contact area (WL) can grow and shrink as the water table rises and falls [e.g., *Hewlett and Hibbert*, 1963; *Dunne and Black*, 1970a, 1970b], making RC a dynamic parameter. But the mean river conductance must reflect the long-term groundwater drainage efficiency, that is, the drainage density of a river basin has evolved to accommodate its long-term drainage need. Hence we define RC as the product of an equilibrium part and a dynamic part that represents deviations from the mean. From setting equation (1) (groundwater mass balance) to equilibrium (left hand side vanishes), assuming no groundwater-floodplain exchange (FG = 0) and combining with equation (6), we obtain the equilibrium conductance as

$$\mathrm{ERC} = \frac{-\Delta x \Delta y R + \sum_{1}^{8} Q_g}{\left(h_{ge} - h_r\right)} \tag{7}$$

where h_{ge} is the equilibrium water table head of the cell from the high-resolution equilibrium results (Figure 1) obtained with climatologic mean recharge. The idea is that long-term groundwater recharge plus lateral convergence from upland cells (numerator) balances long-term river base flow (denominator x ERC), and ERC represents this long-term mean groundwater-river hydraulic connection. We define the dynamic part of RC as

$$\mathrm{DRC} = \exp\left[a\left(h_g - h_{ge}\right)\right]. \tag{8}$$

[29] It is based on the observation that groundwater discharge depends on the water table height exponentially [*Eltahir and Yeh*, 1999]. The idea is that as water table rises, stream channels widen and extend, increasing drainage density and accelerating groundwater discharge; as the water table falls below headwater channels the latter are turned off, decreasing groundwater discharge and forming a negative feedback that dampens the water table fluctuations. The parameter a in equation (8) is assumed to be a sinusoidal function in our earlier work over N. America [*Miguez-Macho et al.*, 2007] to account for drainage density change in a range of terrain slopes. Here for simplicity we assume $a = 1$ over the same range of slopes and $a = 0$ on steep slopes (drainage network does not expand). The product of ERC and DRC gives the RC in equation (6).

3. Model Parameters, Atmospheric Forcing, and Simulation Setup

3.1. Land-Surface Parameters

3.1.1. Land Cover and Soil

[30] Land-cover data is obtained from Global Land Cover 2000 Product by the European Commission Joint Research Center (http://bioval.jrc.ec.europa.eu/products/glc2000/products.php). The S. America map, at <1 km resolution, is produced from four sets of satellite data [*Eva et al.*, 2002, 2004], each better suited to detect certain land attributes; e.g., permanently and periodically flooded forests are from the composite of forest land cover type obtained from ASTR-2 on board ERS-2 satellite and VGT on board SPOT satellite, and surface flooding at high and low waters from SAR on board JERS-1 satellite. It represents the state-of-art land cover data based on the most recent satellite data. We used this data set for assigning the Manning's roughness coefficient (n in equation (4)) for different vegetation covers on the floodplain (e.g., shrub versus forest).

[31] Soil data is obtained from UNESCO's Food and Agriculture Organization (FAO) digital soil map of the world at 5 arc-minute grids (http://www.fao.org/nr/land/soils/digital-soil-map-of-the-world/en/). Fractions of silt, clay, and sand are mapped into 12 texture classes as defined by the U.S. Department of Agriculture (http://soils.usda.gov/education/resources/lessons/texture/). The 12 classes are then assigned hydraulic parameters based on the method of *Clapp and Hornberger* [1978]. The dominant soil types in the Amazon are clay-loam (class 8) and clay (class 11). The soil map is shown in the companion paper where soil moisture and land-surface fluxes are discussed. We note that such a characterization of soil hydraulic properties are far from adequate for realistically representing soil water fluxes. Main issues are that the original soil surveys were of qualitative nature, and that the grid resolution is far too coarse to reflect fundamental pedogenic variations at hill-to-valley

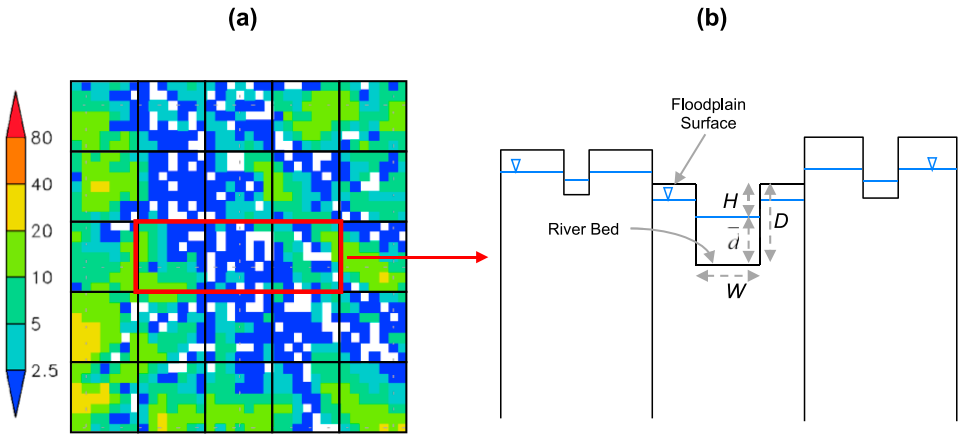

Figure 4. (a) Estimating river and floodplain parameters in a 60 arc-second grid cell (black lines) from the 9 arc-second equilibrium water table depth (background, in m) where the white pixels indicate groundwater emergence and represent perennial rivers. (b) Definition of river and floodplain parameters.

scales. However, addressing these issues requires community-level and international efforts and is beyond the scope of the present paper.

3.1.2. Topography

[32] Topography information is obtained from the digital land-surface elevation data from the U.S. Geological Survey HydroSHEDS data set (http://hydrosheds.cr.usgs.gov/) from NASA Shuttle Radar Topography Mission (SRTM). The product grid of 3 arc-second (~90 m) was aggregated to 9 arc-second (~270 m) for simulating the equilibrium water table [*Fan and Miguez-Macho*, 2010, Figure 1], which is used to initialize the model and define perennial rivers as described later. For the simulation in this study, it is further aggregated to 60 arc-second (~2 km) for computation feasibility, as illustrated in Figure 4a.

[33] We note that HydroSHEDS topography is produced with the combination of two void-filling algorithms, the CIAT algorithm and the HydroSHEDS algorithm. CIAT fills data voids by applying an interpolation, whereas the HydroSHEDS uses an iterative neighborhood analysis. The HydroSHEDS algorithm gives higher weight to low-elevation neighbors to facilitate channel network delineation, but it makes the already low-lying Amazon valley even lower than observed, causing spurious flooding. Thus we use the void-filled product based on CIAT algorithm only, available from the CGIAR-CSI SRTM 90 m Database (http://srtm.csi.cgiar.org).

[34] The land cover data set is used to correct the digital elevation bias on the floodplain and river surface. Since the shuttle radar senses the composite height of the land and the vegetation, the floodplains under forests are artificially elevated, constraining flooding at the forest edge. A comparison between SRTM and ICESat laser altimetry in different topographic and vegetation conditions around the world [*Carabajal and Harding*, 2006] concludes that in vegetated areas, SRTM elevation on average is located ~40 percent of the height from canopy top to the ground, which translates into a 8–30 m with an average canopy height of 20–50 m in the central Amazon [e.g., *Whitmore*, 1992]. We subtracted 20 m from the SRTM elevation at cells mapped as flooded forests in the land cover data set. A similar correction is also performed by *Coe et al.* [2008] who subtracted 23 m for floodplain simulations in the Amazon, and *Cuartas* [2008] who used a linear regression on a watershed near Manaus, which effectively lowered the elevation by ~20 m.

3.1.3. River and Floodplain Parameters

[35] River cells are identified based on the equilibrium water table. The white pixels in Figure 4a (water table at land surface) define locations of persistent groundwater convergence or perennial rivers. Six parameters are defined for each cell: drainage direction (1 of 8 neighbors), river length (L) and width (W), floodplain elevation, long-term mean flow depth ($\overline{d}$) and bank height (H). The latter four are illustrated in Figure 4b.

[36] River flow direction and river length within a cell (L) are obtained using a river network up-scaling method based on *Yamazaki et al.* [2009], from the 15 arc-second USGS HydroSHEDS flow direction file. The method is chosen here because it preserves the network structure and the tortuous river length in the original high-resolution network. Channel width (W) is based on its empirical relationship with drainage area. The classic river hydraulic geometry formula of *Leopold and Maddock* [1953] have been widely applied, but since these empirical relationships are highly site specific [*Singh*, 2003], the formula of *Coe et al.* [2008] based on observations in the Amazon offers a clear advantage. *Coe et al.* [2008] gives

$$W = aA^b \tag{9}$$

where W is in m, A is drainage area (in km^2) above a cell, and a = 0.421and b = 0.592 are empirical constants. The result is shown in Figure 5a for the central Amazon. Compared to field measurements of *Mertes et al.* [1996] at 21 locations along the main stem, the formula gives a slightly narrower channel and monotonic downstream widening while real channels have local reversals. We note that our channel width necessarily simplifies a highly complex natural system in the flat foreland basins and the central valley with multiple channels branching and rejoining (anabranching) and further complicated by their connections with many floodplain lakes [*Richey et al.*, 1989a, 1989b;

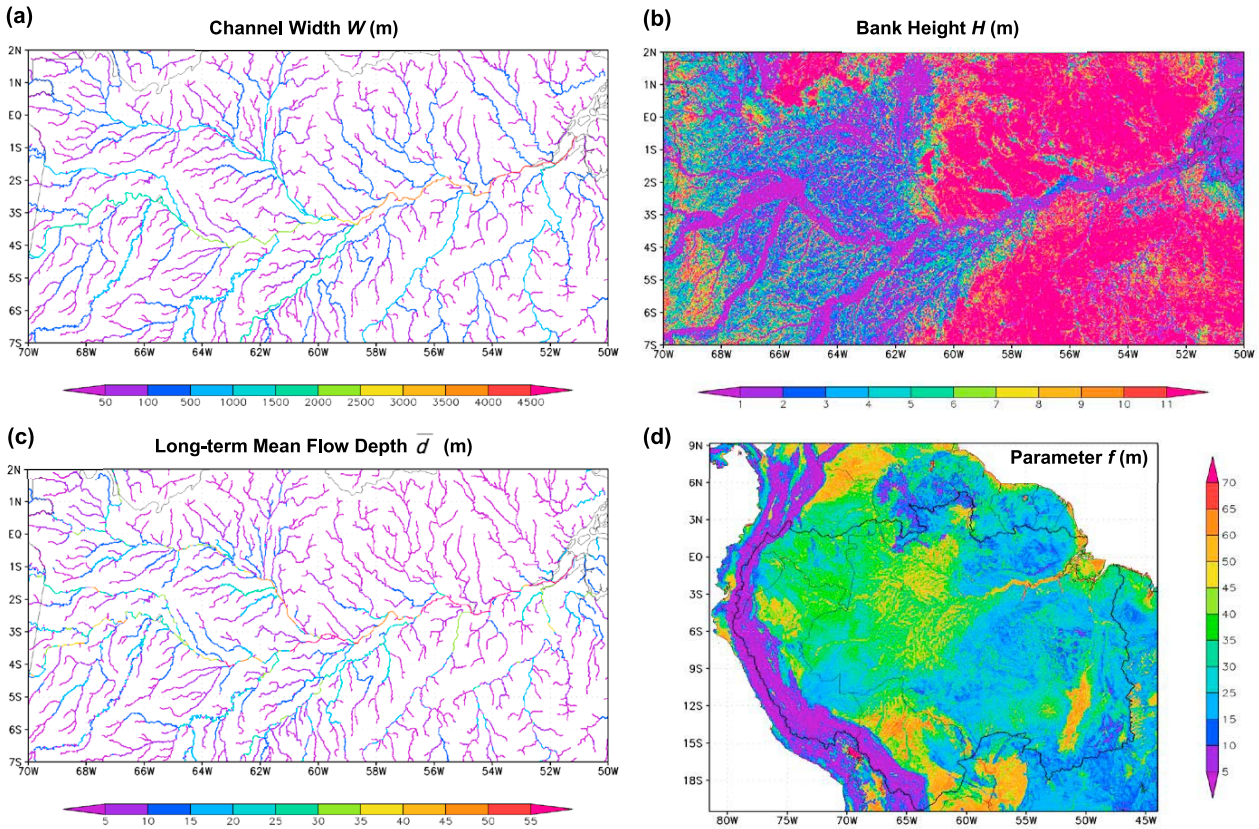

Figure 5. (a) Channel width W (m), (b) bank height H (m), (c) long-term mean flow depth $\overline{d}$ (m), and (d) the e-folding depth of permeability decrease.

Mertes et al., 1996; *Latrubesse et al.*, 2005]. The individual threads of channels cannot be explicitly resolved in a continental-scale model, and we rely on the notion of an 'effective channel' in a given grid that mimics the tasks of the multiple, anabranching channels and lakes.

[37] To define floodplain elevation, we use the high-resolution equilibrium water table as a guide (Figure 4). For each cell in Figure 4b, the mean land elevation of white pixels (water table at land surface) represents the equilibrium river surface elevation, and the mean of the rest of the pixels represents floodplain elevation. Where there are no white pixels, i.e., groundwater emergence is not resolved at the 60 arc-second grids, river surface and floodplain have the same elevation. However, such averaging, plus corrections for forest canopy height discussed earlier (subtracting 20 m if land cover is flooded forest), resulted in a bumpy profile along the valleys, exacerbating numerical instability in flood routing. The following steps are taken to smooth the valley topography. First, a five-cell moving average is applied along the channel profile of wide rivers (>180 m wide, ~2 pixels in the 3 arc-second HydroSHED product) because they have gentle bed slopes and large inertia. Second, the downstream descend is made monotonic by lowering the artificial dams to the same elevation of their upstream cells, starting with the wide rivers followed by the tributaries from the junctions upstream. This is done repeatedly until all dams and sinks are eliminated. However, it results in long river stretches at the same elevation forming steps. Third, this is corrected by interpolating between the end points of each long, flat stretches, again starting with the wide rivers from the base level at the ocean upstream, followed by the smaller tributaries from the junctions upstream, making sure that the slope is >1e-6 for numerical stability (a low value compared to the observed 0.00002 near Manaus [*Meade et al.*, 1991]). This three-step procedure is performed first for the river surface elevation and then for the floodplain elevation, making sure that the floodplain in the cell is always at or above the river surface elevation.

[38] The river bank height H, measured above the mean flow depth (Figure 4b), is a key parameter controlling flood frequency and extent, and is commonly a tuning parameter in large-scale routing models referenced earlier. Here it is obtained as the difference between the floodplain elevation and the river surface elevation in the cell, both based on high-resolution HydroSHED topography product with the correcting and smoothing described above. Where this difference is small, such as on the floodplain, floodwater spreads easily, and where it is large, such as at the edge of the floodplain and in narrow tributary valleys, floodwater is contained. The resulting bank height is shown in Figure 5b. It strongly reflects the topography and the underlying geology; e.g., in the Guyana and Brazilian Highlands flanking the mid-lower Amazon, rivers are cut into the bedrocks, and the banks are high (Figure 5b, magenta color), restricting flooding extent; in the flat foreland basins of the upper Amazon and along the Solimoes, rivers generally deposit sediments [*Kalliola et al.*, 1991, 1992; *Mertes et al.*, 1996; *Dunne et al.*, 1998; *Aalto et al.*, 2003; *Latrubesse et al.*,

2005], and the banks are low (Figure 5b, purple color) and flooding spreads laterally. This method avoids tuning this sensitive parameter as routinely done in continental-scale river routing models.

[39] *Coe et al.* [2008] derived a formula for channel depth (D) similar to that for channel width (equation (9)), but in numerous river sections it is too shallow to contain the mean annual river discharge $\overline{Q}$ if the formula for river width in equation (9) is used. For this reason we take a different approach, whereby channel depth (D) is obtained as the sum of the mean flow depth ($\overline{d}$) and mean bank height (H) as shown in Figure 4b. The long-term mean flow depth ($\overline{d}$) is inferred from Manning's formula (equation (4)) by replacing the hydraulic radius (HR) with mean flow depth ($\overline{d}$), the friction slope (S_f) with the longitudinal channel slope (S), and long-term mean discharge ($\overline{Q}$) in relation to mean flow velocity ($\overline{v}$) and cross-sectional area ($W\overline{d}$)

$$\overline{d} = \left(\frac{\overline{v}n}{\sqrt{S}}\right)^{3/2}, \overline{v} = \frac{\overline{Q}}{W\overline{d}}. \tag{10}$$

[40] The mean flow depth ($\overline{d}$) can be solved iteratively from equation (10), where $\overline{Q}$ is obtained as long-term mean P-ET from ECMWF-Interim Reanalysis (our forcing) over the drainage area above a cell. The advantage is that the resulting mean flow depth (Figure 5c) is compatible with channel width and slope in conveying the mean discharge, because it depends on the latter through equation (10).

3.1.4. Groundwater Parameters

[41] A key parameter for computing lateral groundwater flow (Q_g, equation (1)) is the hydraulic conductivity K [L/T] of the sediments, unknown below the depth of the global soil data set (1 m). Lacking a better alternative, we adopt common assumptions in its vertical distribution. Porosity and permeability of the earth's crust are known to decrease with depth, and at kilometer scales, the decrease appears exponential [*Manning and Ingebritsen*, 1999; *Rojstaczer et al.*, 2008]. In hydrologic modeling which generally includes the weathered horizon only, an exponential profile is also widely assumed [e.g., *Beven and Kirkby*, 1979], which we adopt here

$$K = K_o \exp\left(-\frac{z}{f}\right) \tag{11}$$

where K_o is the known value at the base of the top 1 m from the global soil data set. The value of f in equation (11) which controls how fast the permeability decays with depth, reflects the sediment-bedrock profile, especially the weathering depth, and it has a complex dependence on the climatic, geologic and biotic history at a location. However, terrain slope has been recognized as a first-order control on sediment thickness at continental scales [*Ahnert*, 1970; *Summerfield and Hulton*, 1994; *Hooke*, 2000]; the steeper the terrain, the more erosion over deposition and hence the thinner the weathered mantle. More recent field and modeling studies at hill-to-valley scales [e.g., *Heimsath et al.*, 1997; *Pelletier and Rasmussen*, 2009] suggest that the longitudinal curvature (second derivative of elevation) is a primary control on regolith depth. It is likely that the latitudinal curvature (along contours) may also play a role because it controls water and sediment convergence [*Troch et al.*, 2003]. Although these studies offer exciting opportunities to improve our models in the absence of field characterizations of soil depths, at our grid size of ~2 km, hillslope curvatures cannot be meaningfully defined, and hence we use terrain slope to parameterize f.

[42] We follow the same two-step procedure in our previous work over N. America [*Fan et al.*, 2007; *Miguez-Macho et al.*, 2007]. First, a high-resolution equilibrium simulation is performed where we assume that the drainage of the river network is resolved; this step has been completed in *Fan and Miguez-Macho* [2010]. Second, we aggregate the high-resolution f to obtain the parameter for the lower-resolution simulation that includes fully coupled soil moisture and river dynamics. At the lower resolution, only the large scale lateral flow is resolved, and the internal drainage within each cell is accounted for by the term RG (river-groundwater exchange within a cell, section 2.5 above). To obtain f for the high resolution equilibrium simulation, we proposed a polynomial function with terrain slope, and by trial and error we found the parameters that best reproduced the 568,557 well observations over N. America [*Fan and Miguez-Macho*, 2011]. Because f depends on the slope resolved, it necessarily varies with the grid resolution used, which is why it differed between *Fan et al.* [2007] where the grid size is 1.25 km and *Fan and Miguez-Macho* [2011] where the grid size is 270 m, the same as in the simulation of S. America in *Fan and Miguez-Macho* [2010] pertaining to this work (Figure 1).

[43] The f value can be interpreted as the depth at which the permeability reduces to 1/e (~37%) of the known surface value (K_o). The map of the aggregated f is shown in Figure 5d, where deep sediments (high f) correspond to flat terrain (e.g., Orinoco basin, Peruvian and Bolivian Amazon, Bananal Island, and the Pantanal), and shallow sediments (low f) correspond to steep slopes (e.g., the Andes, and the Sierra de-Maigualida, Venezuela). This broad pattern agrees well with the geologic framework of erosion-deposition balance on the continent [e.g., *Clapperton*, 1993].

[44] The lack of real aquifer information across the Amazon basin and the necessity to rely on simple sediment depth functions (equation (11)) are the main reasons for us to formulate the groundwater flow as simply as possible. Therefore we adopt a two-dimensional flow formulation in LEAF-Hydro-Flood, instead of fully three-dimensional that also calculates the vertical flow component, that is, we only characterize the vertically integrated, lateral groundwater divergence and convergence. This formulation is commonly referred to as the Dupuit-Forchheimer Approximation in groundwater literature [e.g., *Freeze and Cherry*, 1979], widely applied to studying hill-to-valley groundwater drainage problems. It captures the fundamental physics of shallow groundwater movement without relying on parameters that are not available, such as vertical variations in permeability due to complex stratigraphic structures. It also yields an analytical solution for flow transmissivity, which reduces computation, an essential advantage for continental-scale models.

3.2. Atmospheric Forcing

[45] LEAF-Hydro-Flood is forced with ECMWF Reanalysis Interim Product (ERA-Interim, or Interim http://www.ecmwf.int/products/data/archive/descriptions/ei/index.html) [*Dee et al.*, 2011]. It covers the period of 1989 to the present globally on a Reduced Gaussian Grid of N128 (roughly even spacing of ~70 km), with analysis at 00Z, 06Z, 12Z, and 18Z and forecasts at 3 hr steps. Our forcing fields are from

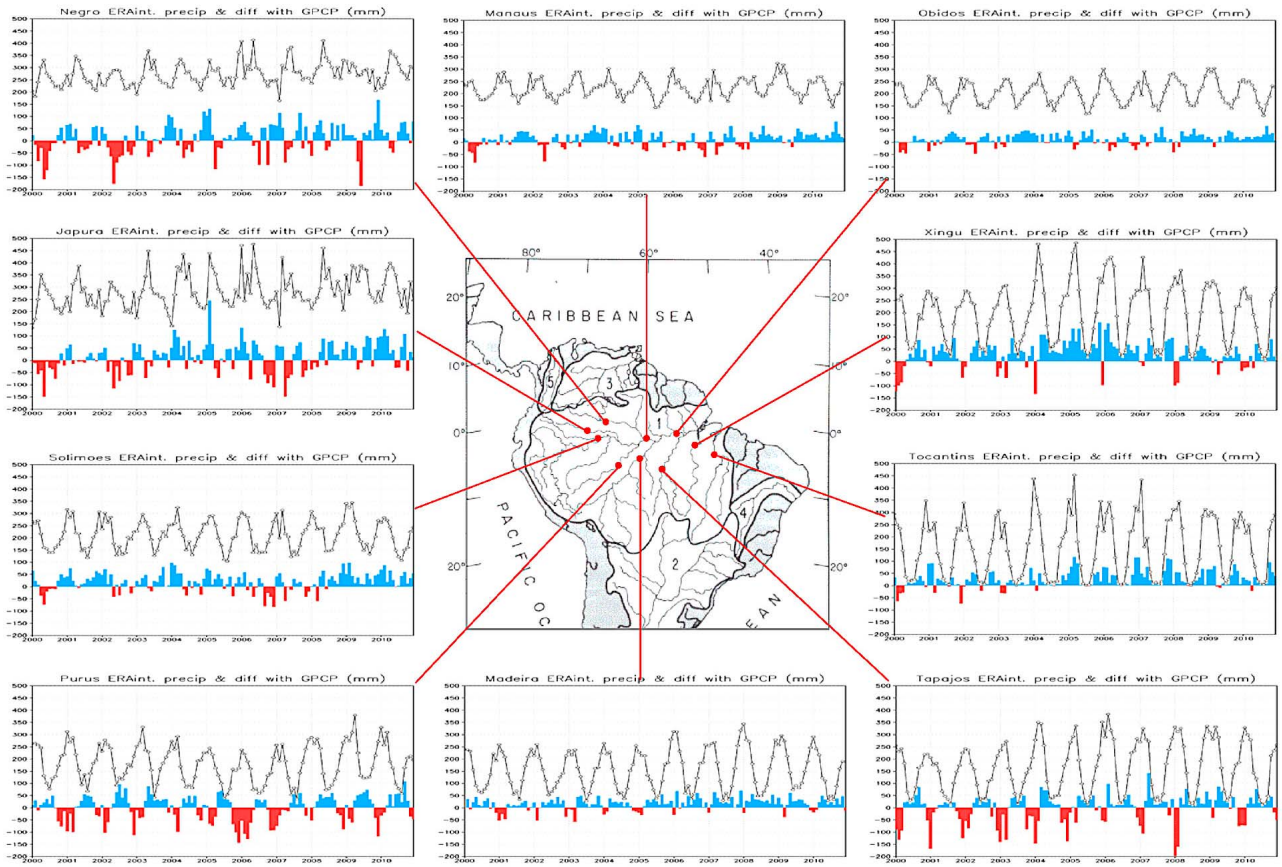

Figure 6. ERA-Interim monthly rainfall (gray) and the difference from GPCP (blue and red) over 10 basins (above 10 river gages) in the Amazon.

the 6 hr analysis for temperature, humidity and wind, and from the 3 hr forecasts for radiation and precipitation to better resolve the event to diurnal changes. Preliminary assessment of ERA-Interim over the whole Amazon [*Betts et al.*, 2009] suggests significant improvement in annual mean precipitation by removing the drying trend in the earlier product, but seasonal amplitude remains too small compared to observations.

[46] We further examine the spatial distribution of Interim rainfall across the Amazon by comparing it with the merged satellite-gage analysis of GPCP (Global Precipitation Climatology Project [*Adler et al.*, 2003]). It is not certain how well GPCP represents the 'truth' given the sparseness of gages in the interior Amazon, the potential biases in satellite estimates, and the product's coarse grid size (2.5°), but a recent comparison among GPCP and other observation-based products over the Amazon [*Juárez et al.*, 2009] suggests that GPCP seasonal rainfall is in close agreement with three other estimates, giving some reassurance. Hence we consider GPCP as closest to the 'truth' for assessing the Interim rainfall forcing. Figure 6 plots the time series of Interim monthly total and its difference from GPCP (bars) over 10 drainage basins used later for model validation, and Figure 7 plots their seasonal climatology (blue lines), giving mean annual rainfall and differences. Two features stand out. First, the Interim is significantly higher than GPCP over the western (Japura, Solimoes, Madeira) and eastern (Xingu, Tocantins) Amazon. Second, the difference follows a seasonal pattern; over the northern and southern basins with large seasonal cycle (Negro, Purus, Madeira, Tapajos) the Interim has less rain in the rainy season and more rain in the dry season. The reduced seasonality is apparent in all basins but Xingu and Tocantins, consistent with *Betts et al.* [2009] that the Interim seasonal amplitude is too small. The higher overall Interim rainfall and its concentration into the dry seasons will directly affect the model water budget, as discussed in detail later.

3.3. Initial Conditions and Model Resolutions

[47] The model domain is the northern 2/3 of S. America (Figure 5d) including the Amazon basin and the adjacent drainage of the Orinoco to the north and the Tocantins to the east, as shown in the center of Figures 6 and 7 (drainage basins 1 and 3). The model resolution is 60 arc-second (~2 km). The initial water table depth is from aggregating the 9 arc-second equilibrium results (Figure 1) to 60 arc-second grids as shown in Figure 4a. The initial soil moisture fields at different depths are obtained as the equilibrium profile by solving the Richard's equation with constant-flux top boundary condition and saturation bottom boundary condition at the initial water table depth; the constant flux is the long-term mean recharge rate used to obtain the equilibrium water table of Figure 1. The resulting top 2 m soil moisture map is given in the companion paper where soil

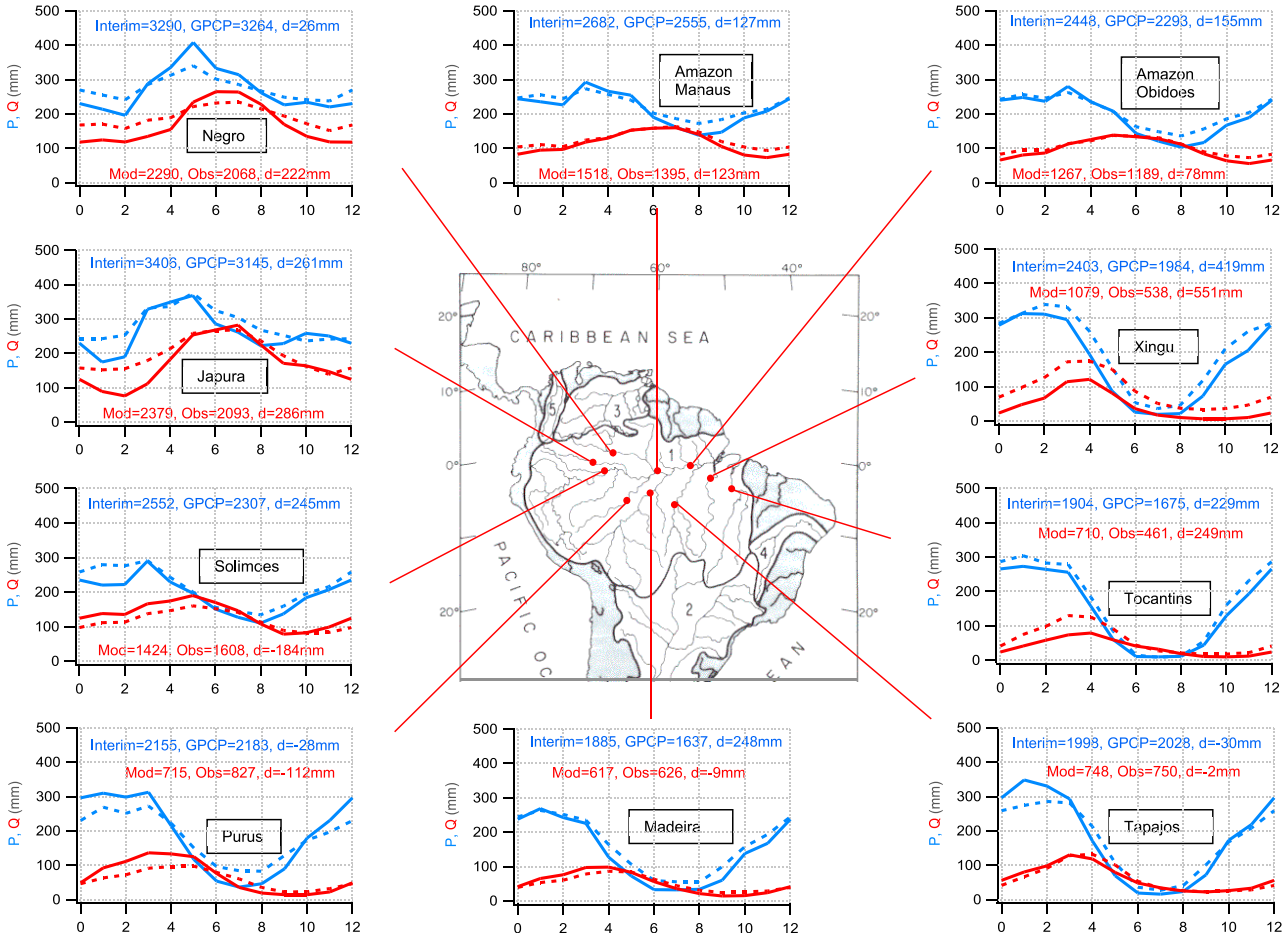

Figure 7. Comparison between mean seasonal precipitation from Interim (blue dash) and GPCP (blue solid) and river discharge forced by Interim (red dash) in this study and observed (red solid) at 10 large gages in the Amazon.

moisture and ET are the focus. The initial surface water storage in river channels and floodplains is obtained from the mean *P* minus ET from HTESSEL land model (same forcing data for the initial water table) integrated over the drainage area above each river cell. Thus the model initial conditions represent a mean hydrologic state of the Amazon system.

[48] At this grid resolution, there are 2250 × 1780 (4,005,000) model grid cells over the domain. To reduce computation we take advantage of the wide range of time-scales from canopy to groundwater response, with canopy and soil integrated at 4 min steps, floodplains at 1 min and rivers at 0.5 min where the full momentum equation is solved (for numerical stability), and water table response and lateral groundwater flow at 20 min steps. The computation takes ~12 h to complete a model year using 186 Itanium Montvale processors of the Finis Terrae supercomputer at the CESGA Supercomputer Center of the Universidade de Santiago de Compostela, Galicia, Spain. Model output is saved at daily steps for all variables as limited by data storage.

4. Model Validations

[49] Here we evaluate the simulations with observed streamflow, water table depth and seasonal flooding. Comparisons with observed soil moisture and ET are given in the companion paper where land-surface fluxes are the focus. Because no parameters are tuned to match observations, the validation here offers independent checks on model performance. Although reproducing observations is not the goal of the study, it provides a reality check on the model's ability to close the water budget in all reservoirs for the right reasons. Hence we devote this section to model validation. We focus on the model's ability to simulate the seasonal dynamics in the surface and groundwater stores in the Amazon, bearing in mind the Interim forcing bias.

4.1. Comparison With Observed Streamflow

[50] Daily streamflow at 10 gages with the least missing data and largest drainage area on major tributaries are obtained from Brazilian Agência Nacional de Águas (ANA, http://hidroweb.ana.gov.br/) over the 11-year period of 2000–2010. Figure 8 plots the daily discharge from observations and simulations, with the mean seasonal cycle given in mm in Figure 7 (red lines). As shown in Figure 7, the rainfall differences between the Interim (blue dash) and GPCP (blue solid) are directly reflected in the runoff differences between the model (red dash) and observations (red solid) except for the Solimoes and Madeira. For example, the small seasonal amplitude in rainfall directly leads to the same reduced seasonable cycle in river flow; and in the

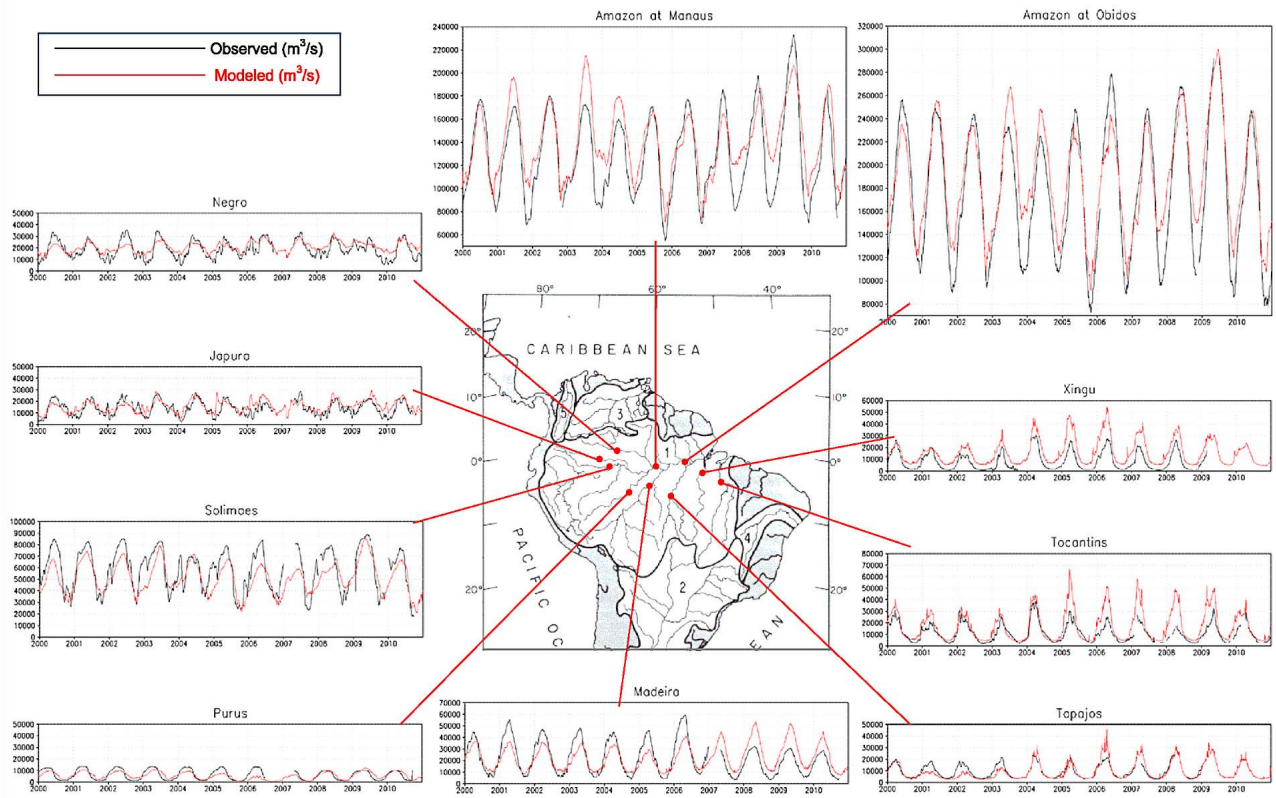

Figure 8. Observed (black) and simulated (red) daily streamflow at 10 gages in the Amazon over 11 years (2000–2010) (discharge in m^3/s).

southeastern Amazon the Interim rainfall surplus (compared to GPCC), mostly in the wet season, is translated directly to increased model runoff (compared to observations). Over the Solimoes and Madeira basins, which drain the Andean eastern slopes, the model wet season runoff is lower than observed despite higher Interim wet season rainfall. It is plausible that here both rainfall products are biased low due to difficulties in resolving steep topography in global models such as the ECWMF model, and sparse rain gages and coarse grids in GPCP. As shown in the companion paper, our model ET is also higher than observed.

[51] We note that at all 10 gages the observations have been corrected by ANA before 2006–2007, with a discontinuity perceptible at some of the gages such as Purus and Madeira (Figure 8) where streamflow is 30% lower in the later years. We also note that hydroelectric dams and regulation of seasonal flow may have affected some of the basins such as Madeira, Tapajos and Tocantins (see http://www.dams-info.org/en).

[52] Overall, we consider the simulated streamflow satisfactory given that no model parameters are calibrated to match the observations. It adequately represents the daily, seasonal, and inter-annual changes in runoff. The seasonal biases are direct responses to the same biases in the rainfall forcing, and the largest discrepancies in runoff correspond to the largest discrepancies in rainfall (e.g., 2003 in Manaus and Obidos, 2005–2007 in Purus, 2005–2009 in Xingu and Tocantins), if one compares the time series in Figures 6 and 8. Over the Amazon above Obidos (excluding Tapajos and Xingu but covering 85% of Amazon drainage), the overall 155 mm higher Interim annual rainfall resulted in 78 mm higher model annual runoff, as reported in Figure 7, partially due to the fact that the extra rain is mostly concentrated in the dry season hence increasing ET in addition to increasing runoff. Finally, the smoothness in the daily time series (Figure 8) suggests that the floodplain storage effect is adequately represented; the daily fluctuations in the Negro and Japura, apparent in both model and observations, are absent in the Solimoes, Purus, and Madeira where large floodplains exist in both the model and the real world.

4.2. Comparisons With Observed Water Table Depth

[53] Eight field studies are found in the literature that report water table depth (WTD) in the Amazon over the model period (Table 1). Except for Rancho Grande and Sinop (site 2 and 6), WTD was observed at more than one topographic location from hilltops to valley floors. Because the exact well locations are not given, and the well spacing is often less than model grid size (~2 km), we organize the observations into two groups, high-ground where the soil is well drained and the groundwater flow is divergent (model hilltops), versus low-ground where the groundwater flow is convergent (model valleys), and chose two corresponding grid cells nearest to the sites.

[54] Figure 9 plots the observed WTD (symbols) at high-ground (red) and low-ground (blue), and the simulated daily WTD (lines), and Table 1 gives the temporal means for the two topographic positions. The mean WTD compares well with the observations, but the seasonal amplitude is too small in the western and northern Amazon (site 1, 3, and 4)

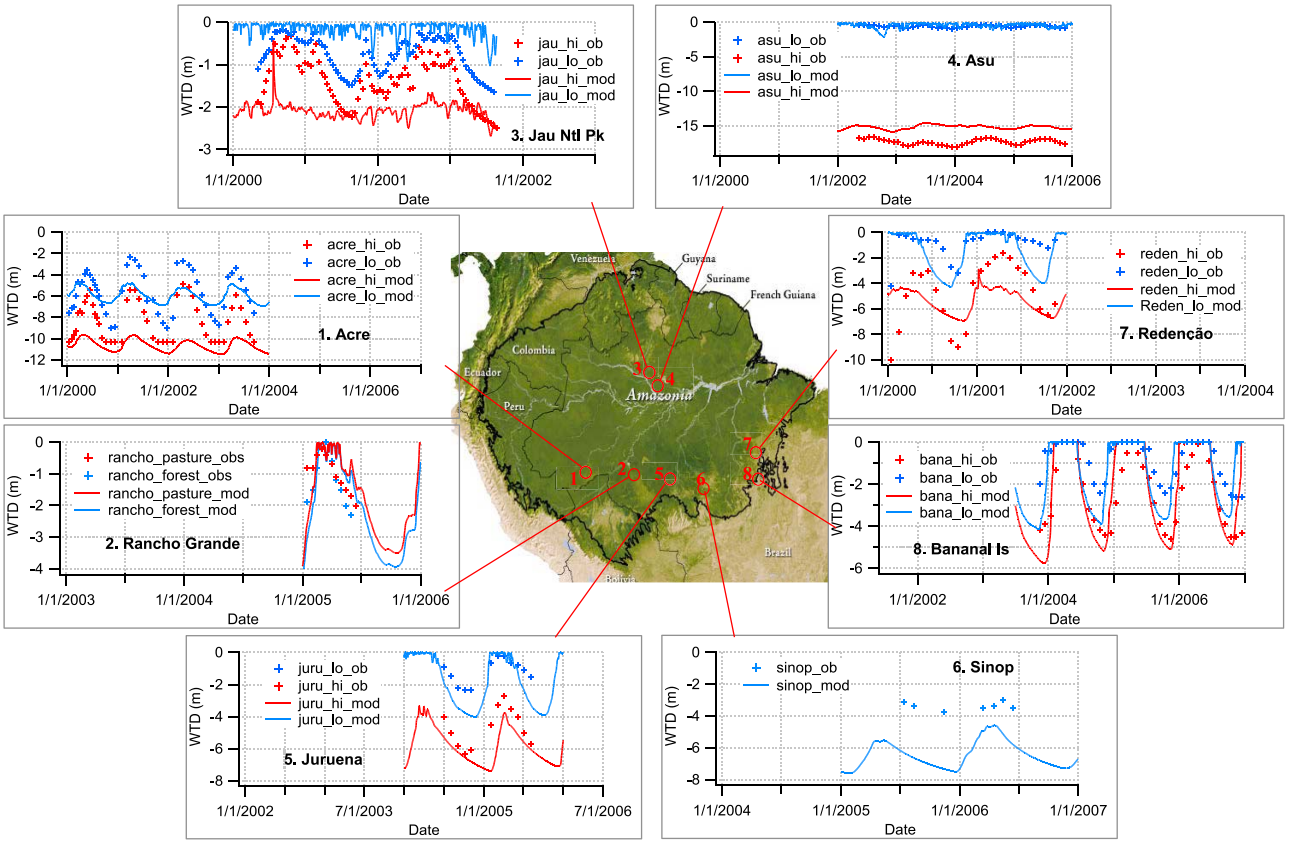

Figure 9. Comparison of modeled (lines) and observed (symbols) WTD (in m) at 8 sites (ordered west to east) at topographic highs (red) and lows (blue). The model grid size is 2 km, but observations are at points (piezometers).

where the small seasonal amplitude in rainfall forcing is apparent (Figures 6 and 7). Another factor is the model soil hydraulic properties that do not reflect the soil at the sites; for example, valley soils are reported as sandy near Manaus (site 3 and 4) which facilitate fast response to infiltration and drainage leading to large water table rises and falls, but the model soil is clay throughout the central Amazon which has low permeability and dampened responses to rainfall forcing.

[55] Given the biases in the Interim rainfall forcing, the lack of adequate soil hydraulic information at high spatial resolutions, and that no parameters are tuned to match observations, we consider the simulated WTD satisfactory in the mean and seasonal dynamics (timing and magnitude).

4.3. Comparison With Observed Surface Flooding

[56] The extent of seasonal surface flooding over the Amazon has been mapped from satellite images by several investigators [e.g., *Hess et al.*, 2003, 2009; *Prigent et al.* 2007; *Papa et al.*, 2010]. The products of *Prigent et al.* [2007] and *Papa et al.* [2010], based on multiple satellites each offering unique advantages, provide a dynamic view of seasonal and inter-annual variations, but they cannot capture the small, isolated patches of flooding and flooding under forest canopy, due to the sensors' coarse resolution (0.25° grid) and inability to penetrate forest canopy. We thus use the flooding extent map produced by *Hess et al.* [2003, 2009] based on radar backscatter from SAR (on board JERS1 satellite) capable of detecting flood under canopy, and at the high resolution of 100 m. Two fly pass radar images, one at high water (1995) and the other at low water (1996) were supplemented and validated with videography at high and low stages a year later (1996 and 1997 respectively). Human interpretation was involved to include pixels likely flooded but missed by the infrequent flybys. These maps are thus interpreted by *Hess et al.* [2003] as the maximum flooding extent.

[57] Figure 10a gives the model simulated flooding frequency as the number of months per year with any surface flooding, averaged over the later 10 yrs of the 11 yr simulation period (2001–2010, discarding 2000). It agrees well with the map of maximum flooding extent by *Hess et al.* [2009] for the Amazon basin below 500 m elevation (not shown). Figure 10b gives the simulation details over the central Amazon, which also agrees well with the map of *Hess et al.* [2003] over the same region. *Melack and Hess* [2011] estimated that flooding occurs over 14% of the basin area below 500 m, and our simulation suggests 18.2%; *Hess et al.* [2003] estimated that this fraction is 17% in the central Amazon box shown in Figure 10b, and our simulation suggests 19.6%. It is expected that more flooding is likely to be experienced over a 10-year period than captured by infrequent fly passes. These comparisons suggest that the model floodplain dynamics is realistic given that no parameters are calibrated to match any of the observations.

[58] In summary, comparisons with observed streamflow, water table depth, and flooding extent suggest that the model

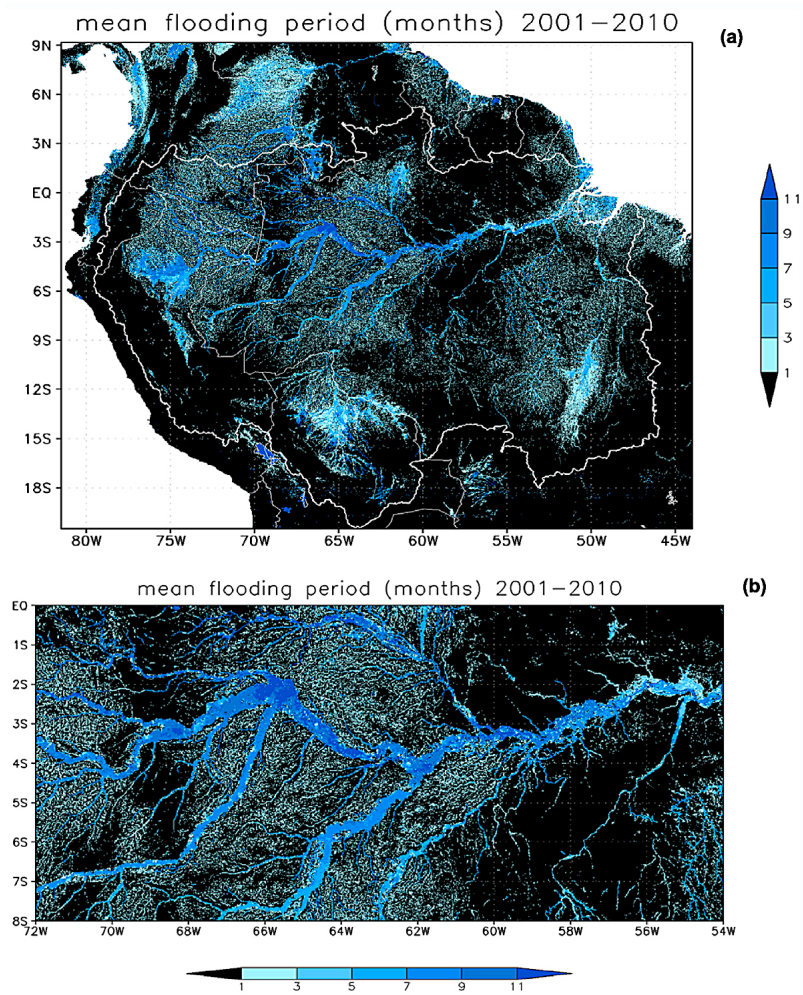

Figure 10. Simulated flooding frequency as number of months per year over the 10-year period of 2001–2010), with (a) over the entire model domain, and (b) over the central Amazon floodplain, all at 2 km grids.

captures the key spatial-temporal features of the Amazon surface and groundwater dynamics. The simulation results have an overall wet bias in the dry season as a result of a similar bias in the Interim rainfall forcing. Potential biases in other forcing variables, given in the companion paper, also played a minor role. A key question is how the bias will affect our investigation into groundwater's role in regulating surface water dynamics. Because the answer is not simple, we take two measures to address the issue. First, we will conduct a parallel simulation without groundwater, but with a free drainage prescribed at the bottom of the model soil column (4 m deep everywhere), with everything else equal. Both runs will be subject to the same forcing bias. Free drainage is the standard approach in current land models, where soil drainage is determined by the hydraulic conductivity at the base of the soil column, uninhibited by the shallow water table. Furthermore, the drained water is placed in the river network instantaneously and routed out to the ocean, unavailable for dry season use later. We will call this simulation the free-drain run, or FD run, and the coupled simulation using LEAF-Hydro-Flood the groundwater run, or GW run. By contrasting the results from the two experiments and focusing on the difference, we hope to isolate the role of the groundwater since both are subjected to the same forcing biases. Second, we will refrain from emphasizing the simulated quantities, and will remain qualitative by focusing on the mechanism, direction and timing of the interactions.

5. Results: Groundwater Influence on Amazon Surface Water Dynamics

[59] We test the basin-scale significance of the four mechanisms posed earlier whereby the groundwater regulates the seasonal dynamics of the Amazon surface waters. To reduce the effect of model spin-up, we leave out the first year (2000) and use the simulation results from the later 10 yrs (2001–2010) where the mean seasonal cycle is the focus.

5.1. Mechanism-1: Groundwater Regulates Streamflow Partition in Headwater Catchments

[60] Observations suggest that in the headwater catchments across the Amazon, groundwater is the dominant

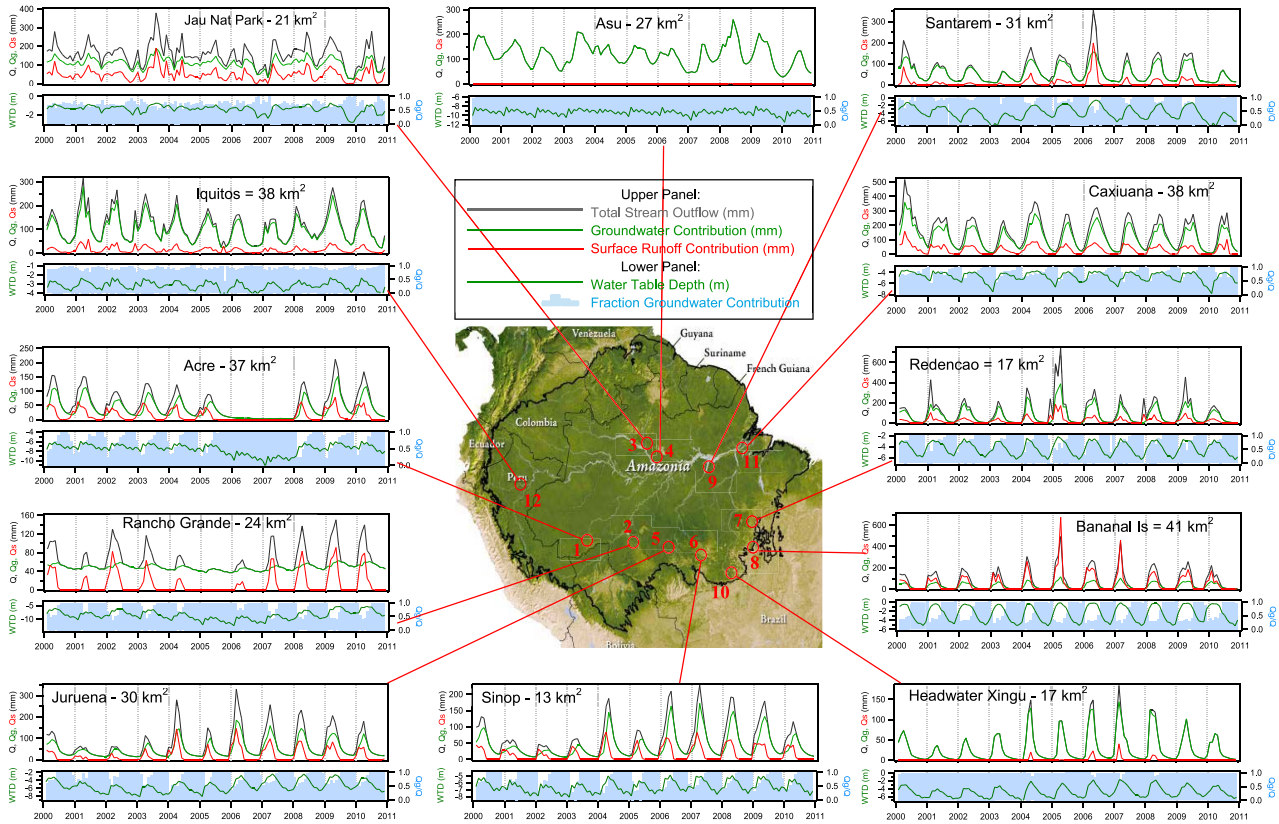

Figure 11. Time series of streamflow (Q), contribution from the groundwater (Qg) and surface runoff (Qs), mean water table depth (WTD), and fraction of groundwater contribution to total streamflow (Qg/Q) from 12 headwater catchments across the Amazon.

source of stream flow, but the magnitude varies from one place to another. Here we provide a synthesis and a mechanistic interpretation that the observed variability can be caused by the varying water table depth; a shallow water table enhances saturation-excess (or Dunne) surface runoff, reducing the relative contribution from the groundwater.

[61] We chose 12 small catchments across the Amazon (Figure 11) that are documented in detailed field studies, including the eight groundwater validation sites (Figure 9 and Table 1), a site with flux tower and soil tracer data [e.g., *Romero-Saltos et al.*, 2005] near Santarem (site 9), two sites with fluvial carbon flux measurements (Headwater Xingu, site 10 [*Neu et al.*, 2011], and Caxiuana, site 11 [*Carmo et al.*, 2006]), and a biodiversity site near Iquitos, Peru [*Lähteenoja and Page*, 2011] (site 12). By choosing these documented field sites we hope to provide a framework to synthesize the observed variations in groundwater-stream links across the sites. The catchment area ranged from 13 to 41 km^2 (given in Figure 11) based on the smallest model-definable drainage basin enclosing the field sites. We note that our ~2 km grid size cannot adequately resolve the hill-valley gradients and the first-order streams as desired; rather, these 12 catchments represent the lower end of the scale-range of the model which we hope will shed lights on the hydrologic behavior of small catchments as close as possible to the instrumented watersheds given the computation limits today. Hence the results need to be interpreted with caution and only in the qualitative sense.

[62] Figure 11 plots the monthly total streamflow (in mm) from these catchments separating groundwater and surface runoff contributions (upper panel), and fractional groundwater contribution and catchment mean water table depth (lower panel). The following can be inferred.

[63] First, as documented in water budget studies in small catchments across the Amazon [*Lesack*, 1993; *Leopoldo et al.*, 1995; *Grogan and Galvão*, 2006; *Hodnett et al.*, 1997a, 1997b; *Cuartas*, 2008; *Neu et al.*, 2011], groundwater supports the bulk of the total streamflow despite variations in local climate, topography, vegetation and soil properties, as seen in the fractional groundwater contribution (blue shading) at all sites.

[64] Second, the variations in groundwater contribution across the sites can be well explained by the water table depth. In order for groundwater to contribute to streamflow, the water table in the catchment has to be above the river height; however if the water table is too shallow, it creates saturation near the valley where rain runs off directly to channels, increasing the relative contribution of surface runoff. At the 12 sites across the Amazon, the water table is above the valley floor all year-round and hence the groundwater is almost always feeding the streams. The question here is whether it is too shallow as to cause saturation and surface runoff. At one end of the spectrum is the Asu watershed near Manaus (site 4), where the deep water table under the plateaus facilitates efficient soil drainage so that surface

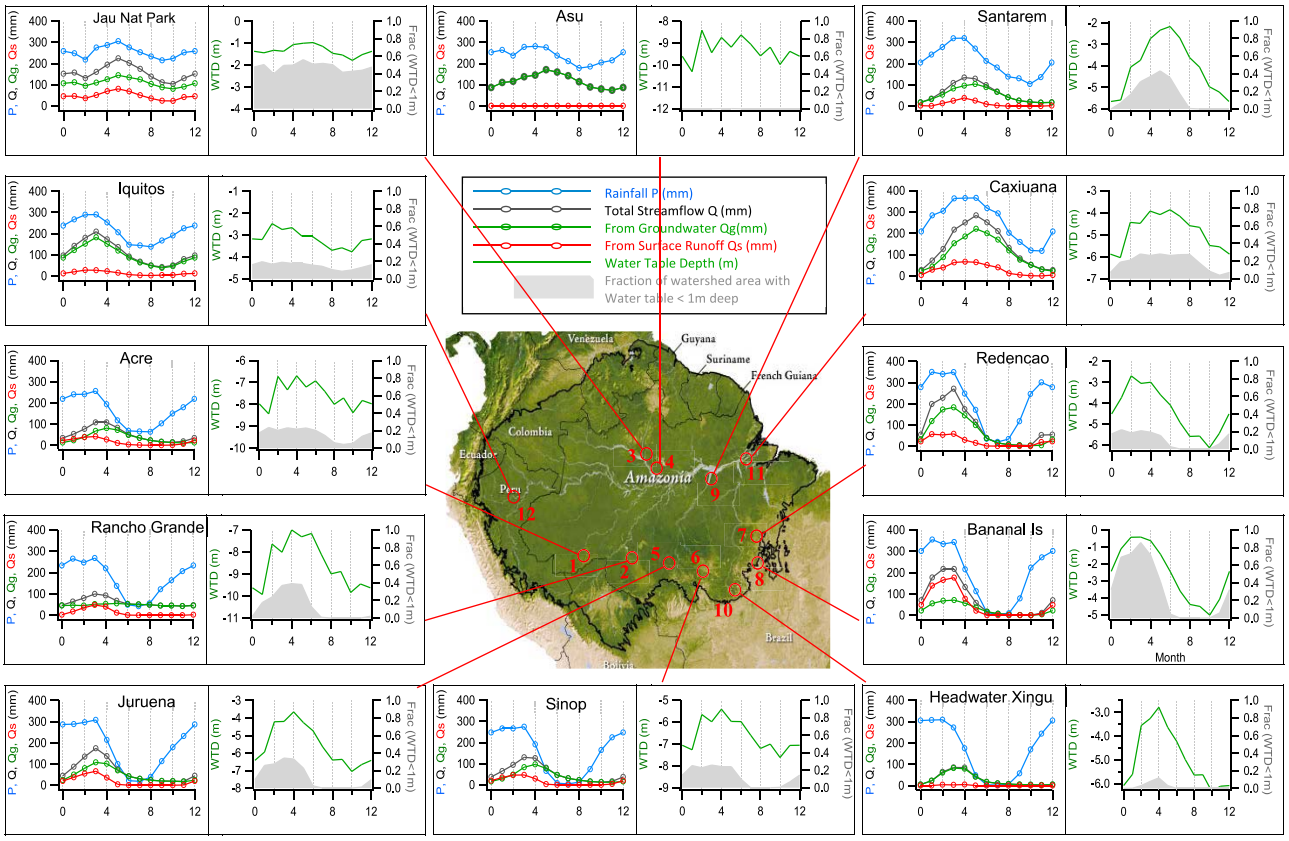

Figure 12. Seasonal cycle of streamflow partitioning and fraction of watershed with shallow water table (shaded) in 12 headwater catchments across the Amazon.

runoff is rarely observed and groundwater supplies nearly the entire streamflow [*Hodnett et al.*, 1997a, 1997b; *Cuartas*, 2008; *Tomasella et al.*, 2008]. The lack of surface runoff is also noted at Santarem (site 9) [*Nepstad et al.*, 2002] and Headwter Xingu [*Neu et al.*, 2011], as simulated by the model. At the other end of the spectrum is Jau Nation Park (site 3) where the water table remained shallow [*Do Nascimento et al.*, 2008], creating saturated valleys where surface runoff occurs.

[65] Third, the relative groundwater contribution is greater in the dry season at all 12 sites, most notably at the southern and eastern sites where rainfall is more seasonal. At these sites, groundwater supports the entire river flow for a few consecutive months in the late dry season. Groundwater storage, filled in the wet season and slowly released in the dry season, is the reason that these streams do not run dry despite multimonth rainfall shortages. (We note that at the Bananal Island site, surface runoff exceeds total river discharge in two years when the Interim rainfall is particularly high (Figure 6, Tocantins, year 2005 and 2007), because floodwater leaves the basin over the wide floodplains without passing the channel outlet.)

[66] These points are further brought out by the mean seasonal cycles shown in Figure 12; added to this plot are mean seasonal rainfall in the left panels (blue) and the fraction of catchment area with shallow water table (<1 m) (shading, right panels). The latter indicates the area of the catchment where surface runoff likely occurs; the shallow water table can quickly rise to the surface in response to local rainfall and upland groundwater drainage, causing valley saturation and the so-called "saturation-excess runoff" (Dunne runoff) common in a humid climate, in contrast to "infiltration-excess runoff" (Horton runoff) common in arid regions. Figure 12 suggests that seasonal saturation occurs in at least a part of the catchment. While half of the catchment near Jau (site 3) can be saturated all year-round (here very likely exaggerated by the high overall but particularly dry season Interim rainfall), large seasonal swings occur at Bananal Island (site 8) where rainfall and saturation fraction are highly seasonal and the landscape alternates between floodplains and dry savannas [*Borma et al.*, 2009].

[67] The idea that in a humid climate surface runoff only occurs over the saturated fraction is not new; it has been repeatedly demonstrated by seminal studies of hillslope and catchment hydrology such as *Betson and Marius* [1969], *Dunne and Black* [1970a], *Freeze* [1971], and *Beven and Kirkby* [1979] and many more since. Recognizing this runoff mechanism, many state-of-art land models have parameterized a saturated grid fraction to accomplish this groundwater control, utilizing the elegant TOPMODEL concept [*Beven and Kirkby*, 1979] where the mean climate and local topography are primary drivers of hillslope-catchment moisture redistribution. Although parameterizing a sub-grid saturation fraction has vastly improved large-scale land models, this fraction, as shown in Figure 12, can be highly variable in space and time as dictated by the water table configuration and its seasonal rise and fall [*Hewlett and Hibbert*, 1963; *Dunne and Black*, 1970a, 1970b;

Tanaka et al., 1988; *de Vries*, 1994, 1995; *Eltahir and Yeh*, 1999; *Marani et al.*, 2001]. Building in a prognostic groundwater can further improve our models by capturing this groundwater-induced, dynamic surface runoff mechanism common in humid river basins such as the Amazon.

5.2. Mechanism-2: Groundwater Regulates Two-Way Floodplain-Groundwater Exchange

[68] Observations suggest that in the lower floodplains, there is a dynamic, two-way exchange between the surface floodwater and the underlying groundwater; in the wet season, rainfall and the expanding floodwater infiltrates into the floodplain sediments, but the amount of infiltration loss is inhibited by the rising shallow water table; in the dry season, groundwater seepage feeds floodplain channels, lakes and wetlands. This two-way exchange has been documented at several sites on the Bolivian, Peruvian, and central Solimoes-Amazon floodplains [*Forsberg et al.*, 1988; *Lesack*, 1995; *Lesack and Melack*, 1995; *Mertes*, 1997; *Cullmann et al.*, 2006; *Hamilton et al.*, 2007; *Bonnet et al.*, 2008; *Bourrel et al.*, 2009; *Borma et al.*, 2009]. Here we evaluate the significance of this exchange across the floodplains of the Amazon and how its dynamics are controlled by the difference between floodwater and groundwater heights.

[69] Figure 13 plots the time series of rainfall (blue shade), floodplain infiltration (dark brown), water table depth (green), floodwater height (red), and groundwater seepage (light brown) over the five large floodplains in the Amazon and Orinoco shown in Figure 14d. The water table is shown in both upper and lower plots for each site for easy comparison of seasonal timing among the variables. The mean seasonal cycle over the 10 yr period (2001–2010) is shown in the right panels. We start our discussion with the floodplain in Bolivia, the southernmost and with the strongest rainfall seasonality, as the following sequence of events.

[70] Near the end of the dry season (Jul-Aug, marked 'a' on Figure 13, bottom-right panel), the water table (green) is falling and still supplies the surface store (red) through seepage fluxes (light brown). Slow and steady groundwater seep was observed on this floodplain and suggested as the means to maintain flooding in the back swamps in the dry season [*Hamilton et al.*, 2007]. However, the water table has fallen significantly from its peak, leaving floodplain sediments unsaturated under higher grounds.

[71] As the wet season arrives and rain falls on the dry floodplain, it quickly infiltrates, as seen from the simultaneous rising of infiltration (dark brown) and rainfall (blue shade) marked 'b' on Figure 13. But the infiltration does not raise the water table yet which continues to fall for another 1.5 months, a result of two processes: filling the unsaturated soil pores to field capacity before the infiltration reaches the water table, and increased groundwater drainage triggered by the initial water table rise. The initial rise steepens the hydraulic gradient toward the floodplain channels and accelerates flow to the channels, and it also causes the water table to rise to the surface and seep out at low spots, both effectively dampening the initial water table rise.

[72] As infiltration accelerates due to increasing rainfall (marked 'c'), it outpaces groundwater drainage governed by the difference between groundwater and surface water levels, the latter now higher, causing the water table to begin to rise, ~2 months after the onset of the wet season.

[73] As the water table rises, it quickly fills the sediments, causing widespread saturation on the floodplain. The latter impedes further infiltration (marked 'd') despite the continuously rising rainfall. Most of the rain becomes surface runoff or directly adds to flooding. The close timing among the rise of water table (green), seepage (light brown), and floodwater height (red) points to the water table's role in controlling infiltration and direct seepage contribution to surface flooding.

[74] The water table continues to rise with the slowed infiltration and rainfall. It reaches the maximum (<1 m on average but shallow in low spots) in Mar-Apr (marked 'e'), 1.5 month after the peak rainfall. As the rain dwindles and infiltration diminishes, groundwater drainage becomes the dominant source for floodplain channels, lakes, and non-flooded wetlands in the driest months of the year (back to point 'a' in the previous cycle). Before the groundwater is completely depleted, the next rainy season has arrived. (We note the large shift in the Interim rainfall forcing in 2005 over this region, causing a shift to higher groundwater and surface water stores and increased model runoff in the Madeira shown in Figure 8 earlier.)

[75] The above sequence of events is closely followed by the floodplain of Bananal Island, the second-most seasonal of the five. One difference is that the floodplain here becomes completely dry in the dry season (no seepage and surface water on the floodplain), and the declining water table feeds the hundreds of lakes as observed by *Borma et al.* [2009]. Infiltration exceeds local rainfall in early wet season due to floodwater convergence from outside the box. The same sequence of events is also repeated over the Orinoco, the northern hemisphere floodplain with a slow-tapering wet season (or a weak second peak), giving rise to a weak second peak in infiltration (dark brown).

[76] Over the central floodplains along the Solimoes, the lack of dry season and its low elevation (poor drainage) lead to a shallow water table all year-round over large portions of the floodplain. Infiltration occurred mainly on high grounds and over periods where/when the water table is deeper, as seen in the opposite phase between water table depth and infiltration. Note that infiltration is not in phase with the floodwater height (red) at all, contrary to our expectation that flooding leads to infiltration. Here the water table is a stronger control on infiltration than flooding stage; the latter, indicative of flood extent, matters little because there is no pore space in the sediments. As in Bolivia, the lower portion of the floodplain surface is kept wet in the dry season by steady groundwater seeps. The dynamics over the Peruvian Amazon floodplain, slightly south of the Solimoes with a more seasonal rainfall, is similar because of its similarly low elevation and poor drainage.

[77] In summary, the five large floodplains exhibit different groundwater-floodplain exchanges in magnitude and phase relations but a common feature emerges; that is, the water table is the primary control on floodplain infiltration, more than the flooding stage is. Furthermore, groundwater keeps the lower spots of the floodplain wet in the dry season in the Bolivia, the Solimoes, and the Peruvian Amazon floodplains as observed. We note that the amount of groundwater seepage is very small compared to infiltration (by 2 orders of magnitude) suggesting the filling of a large floodwater storage in the sediments (in addition to the

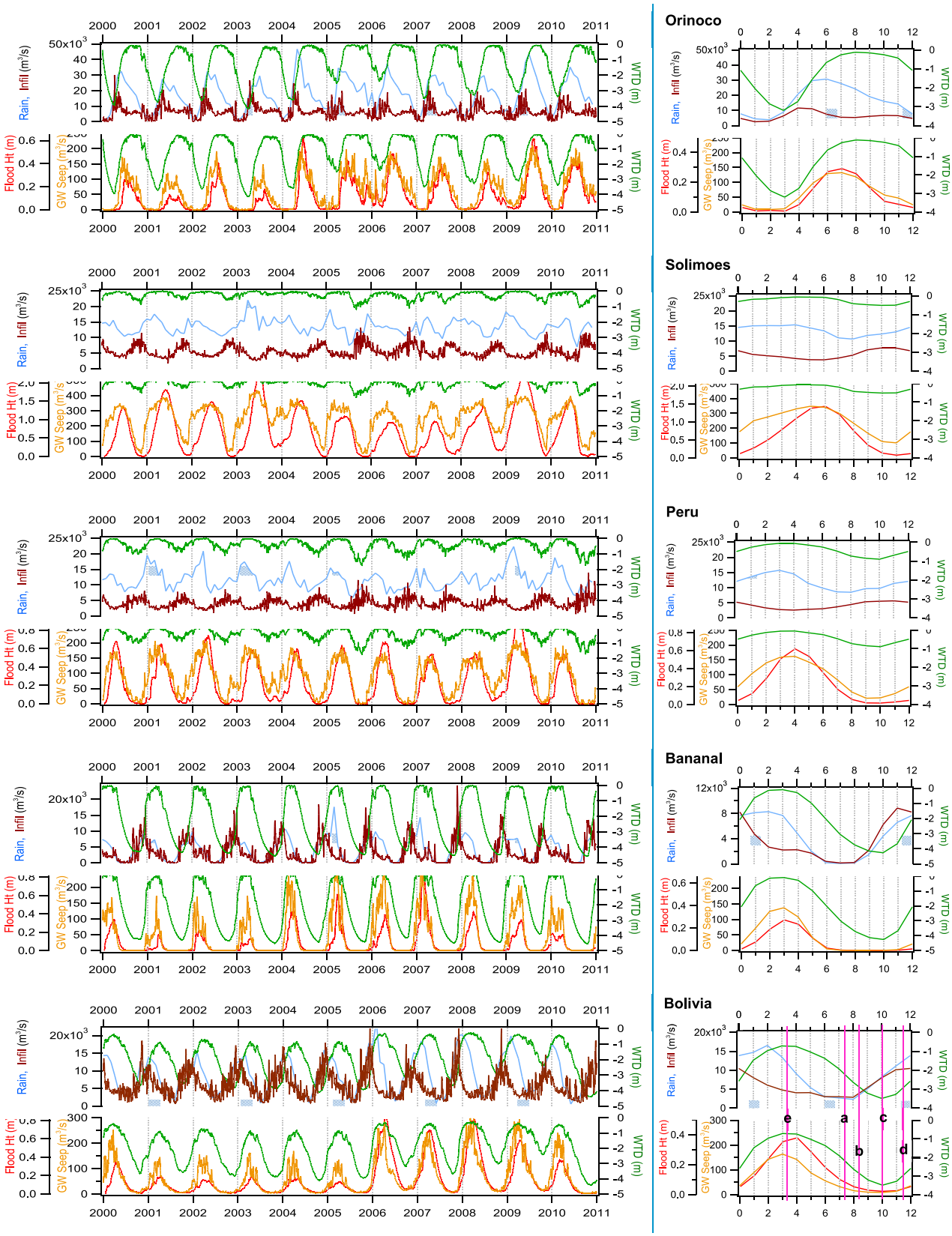

Figure 13. Monthly rainfall (blue shade), daily floodplain infiltration (dark brown), water table depth (green), groundwater seepage (light brown) and floodwater height (red) over five large floodplains in Figure 14d. Mean seasonal cycle is shown to the right.

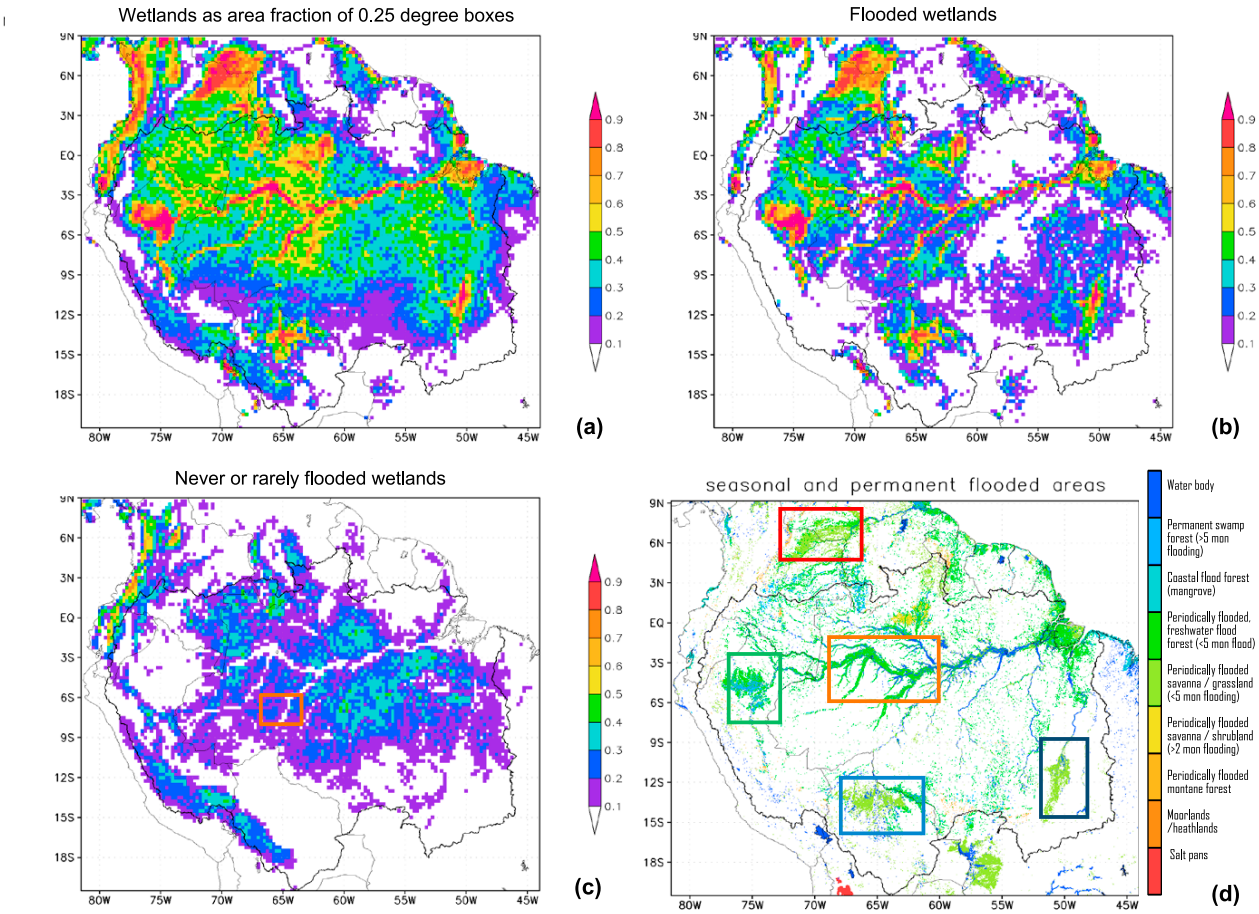

Figure 14. (a) Simulated wetland distribution as area fraction of 0.25 degree cells based on simulations at 2 km grids, (b) wetlands with >1 month of flooding each year, (c) wetlands that are never or rarely flooded (<1 month each year), and (d) flooded land cover types in the European Commission Land Cover Data set [*Eva et al.*, 2002], with locations of floodplains analyzed in Figures 13 and 15.

widely recognized surface storage) earlier in the wet season, further augmenting the storage effect of floodplains.

[78] Floodplain-groundwater exchange is not currently represented in state-of-art global river routing and flooding models, yet this exchange can have important hydrologic and geochemical implications. Although in the Amazon this flux is small, as inhibited by the shallow water table characteristic of humid lowland basins of the world, in drier regions where the water table is deeper, river and floodplain leakage into the underlying groundwater is an important surface water loss term and the main mechanism for groundwater recharge. This is documented in the two largest floodplains in Africa. In the Okavango Delta in Botswana, 80–90% of the seasonal floodwater infiltrates the ground, recharging groundwater and sustaining dry season wetland ecosystems [e.g., *McCarthy*, 2006; *Bauer et al.*, 2006]. In the Sudd where the Nile River tops its banks annually, floodwater infiltrates into the ground to recharge the groundwater as evidenced by the large seasonal cycle in water table depth [e.g., *Mohamed et al.*, 2006]. The importance of enabling this two-way floodplain-groundwater exchange is also noted by *Yamazaki et al.* [2011] as one of the future directions of model development, if our models are to be capable of simulating the whole spectrum of floodplain dynamics in the world without tuning parameters region by region.

5.3. Mechanism-3: Shallow Water Table Supports Non-flooded Wetlands

[79] We test the role of groundwater as a direct support for wetlands rarely under floodwater but characterized by a persistently shallow water table residing in the root zone, creating water-logged soil conditions defining wetlands. Wetlands do not need to be flooded; the water table depth under wetlands reported in the recent literature ranged from land surface to 1.5 m depending on vegetation types and their rooting habits [*Fan and Miguez-Macho*, 2011]. The water table depth is a strong regulator of methane emission from wetlands and required for process-based methane flux models as a key hydrologic forcing [e.g., *Walter and Heimann*, 2000]. Here we evaluate the potential significance of groundwater-supported wetlands which may constitute a methane source in addition to the flooded wetlands observable from space [e.g., *Hess et al.*, 2003; 2009].

[80] Wetlands are defined by saturated soil conditions for at least a part of the growing season as to harbor vegetation

specialized in coping with anoxic soil conditions. Wetland delineation based on hydric soil mapping is not available at the basin scale, and we use the water table depth (WTD) as an indicator of soil saturation. The climatologic mean WTD is shown to be a good indicator of wetland conditions in North America [*Fan and Miguez-Macho*, 2011]. Here we further take into account of the strong seasonality in the Amazon and define wetlands as grid cells where WTD is in the shallow root zone (e.g., 0.25 m) for at least part of the year (e.g., 3 mon) averaged over the 10 yr model period. We note that varying the threshold WTD or wetting duration will result in different estimates of wetland extend, and hence our discussion will remain qualitative.

[81] Because of the patchy nature of small wetlands, it is difficult to present the full ~2 km grid resolution over the whole Amazon, and we plot in Figure 14a the fractional area of 0.25 degree cells, each containing 15x15 model grid cells, that is occupied by wetlands, as is typically done in global and continental wetland maps. By this definition, Figure 14a suggests that much of the Amazon contains some fraction of seasonal wetlands in the river valleys, but we remind the readers that the high rainfall bias and the resulting wet bias in the model may have exaggerated the model wetland area, and the results are to be interpreted with caution. To examine the groundwater's role as a direct support for wetlands, we separate the flooded wetlands (at least 1 mon per year with floodwater) shown in Figure 14b, from the rarely flooded wetlands (less than 1 month a year) shown in Figure 14c. The procedure is illustrated in Figure 15. For comparison, we also show the map of flooded land cover types in Figure 14d from the European Commission Land Cover Data sets [*Eva et al.*, 2002]. We infer the following from these maps.

[82] First, the areas with the most frequent shallow water table (red colors in Figure 14a) correspond closely to the areas of most frequent flooding (Figure 14b), that is, there is a high correlation between flooding and shallow water table. The poor drainage both above and below the land surface at these locations is the primary cause, but there is a secondary cause, that is the feedback between the floodwater and groundwater stores. As shown in the earlier section, floodplain infiltration raises the water table below, and the shallow water table prevents further infiltration loss in the wet season and supplies flooding by seepage in the dry season. This two-way exchange replenishes one another and increases the duration and frequency of full storage in both reservoirs.

[83] Second, the area with the most frequent flooding over the 10 yr model period (Figure 14b) corresponds closely to area of flooded land cover types (Figure 14d) from the European Commission Land Cover Data sets [*Eva et al.*, 2002] as well as the flooded wetland mask of *Hess et al.* [2009] (not shown), both primarily based on surface flooding observed by satellite radar fly passes during 1995–1996. The close agreement between Figures 14b and 14d suggest that the model simulation may be used to supplement the snapshot images; the model's high spatial and temporal resolution (~2 km, 4 min) and time span (10 yrs) can provide insights into the spatial (northern-southern flip) and temporal (daily, seasonal, to inter-annual) variability of flooded wetlands.

[84] Third, there may be areas in the Amazon that experience wetland conditions at least seasonally (>3 mon) but are rarely flooded (<1 mon), as shown in Figure 14c. This map is obtained by removing the flooded wetland pixels at the 2 km grids before calculating the area fraction (illustrated in Figure 15). It suggests that wetland conditions, albeit discontinuous in space and seasonal in time, may be common features in the Amazon landscape. It may also occur in only a small fraction of a catchment, along river corridors forming narrow riparian wetlands and gallery forests in the drier fringes of the Amazon, and in the interior swamps away from major channels but fed by groundwater seeps, all suggested by observations discussed earlier. However, due to the wet-bias in the Interim rainfall forcing, the wetland areas is likely over-estimated. The results here only serve to suggest that groundwater-fed wetlands, difficult to observe from the space, may not be negligible in the Amazon, and targeted, large-scale field investigations are warranted.

[85] Figure 15 gives the flooded and non-flooded wetlands over a 2 × 3 degree box (Figure 14c) at the full model resolution of 2 km, showing the spatial details of possible wetland distribution as suggested by the model.

5.4. Mechanism-4: Groundwater Buffers Seasonal Dynamics of Surface Waters

[86] Last, we examine the time-scale interactions between the slow groundwater and the fast surface waters. Observations in the headwaters of the Amazon [*Hodnett et al.*, 1997a, 1997b; *Johnson et al.*, 2006a; *Grogan and Galvão*, 2006; *Cuartas*, 2008; *Vourlitis et al.*, 2008; and *Tomasella et al.*, 2008] and the lower floodplains [*Forsberg et al.*, 1988; *Lesack*, 1995; *Lesack and Melack*, 1995; *Mertes*, 1997; *Cullmann et al.*, 2006; *Hamilton et al.*, 2007; *Bonnet et al.*, 2008; *Bourrel et al.*, 2009; *Borma et al.*, 2009] suggest that the longer time scales of groundwater can regulate river flow and surface flooding dynamics; because of its delayed and muted response to rainfall, groundwater seepage may persist in the dry season, feeding rivers and wetlands and floodplain lakes.

[87] Groundwater as a dry season water source has been brought out through the earlier discussion in both the headwaters and the large floodplains (Figures 11–13). In Figures 11 and 12, groundwater is shown to support the entire streamflow in late dry season in small catchments in the southeastern Amazon where seasonality is strong. In Figure 13, it is shown that the water table under the large floodplains has a 1–2 month delayed response to rainfall, and groundwater seeps continue in the dry season and often into the next wet season. Here we seek further insights by contrasting the results from the coupled groundwater-surface simulation (GW run) with that from the free drain experiment (FD run).

[88] Figure 16 plots the mean seasonal cycle of river discharge at the 10 large gauges used in the validation (Figures 7 and 8), for both GW (blue) and FD (red). It separates the contribution from groundwater (letter G in line graph) and surface runoff (letter S) to the total discharge. In the FD run, water drains out of the bottom of the 4 m soil column as controlled by the hydraulic conductivity, and is instantaneously placed into the channel storage within a cell. Under the floodplains, the drainage rate is very high, and by instantaneously putting it back into the rivers, just to be drained again after one time step, the FD approach creates an artificial cycle that renders the drainage contribution physically meaningless. Therefore the groundwater contribution

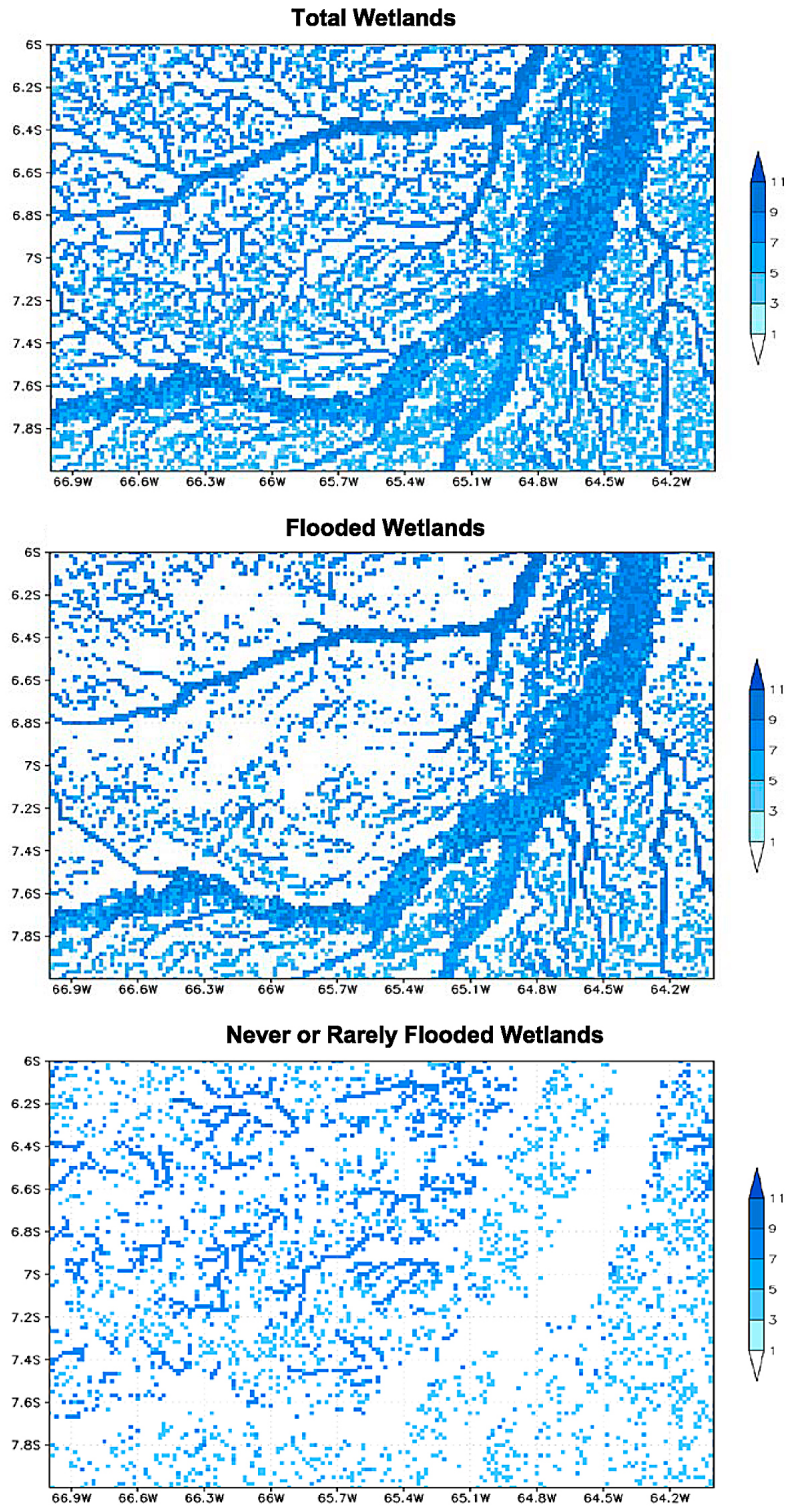

Figure 15. Detailed maps showing (top) total wetlands, (middle) flooded (with >1 month of flooding) and (bottom) non-flooded wetlands in the 2x3 degree box (Figure 14c) at the 2 km resolution. Shades of blue give months with WTD < 0.25 m.

for the FD run is calculated as the total stream discharge minus the surface runoff. Since there is no groundwater storage in the FD run, this approach is valid. The following can be inferred from Figure 16 regarding the total discharge and groundwater versus surface runoff contributions.

[89] Regarding total stream discharge (thick lines without letters), the difference between GW (blue) and FD (red) are

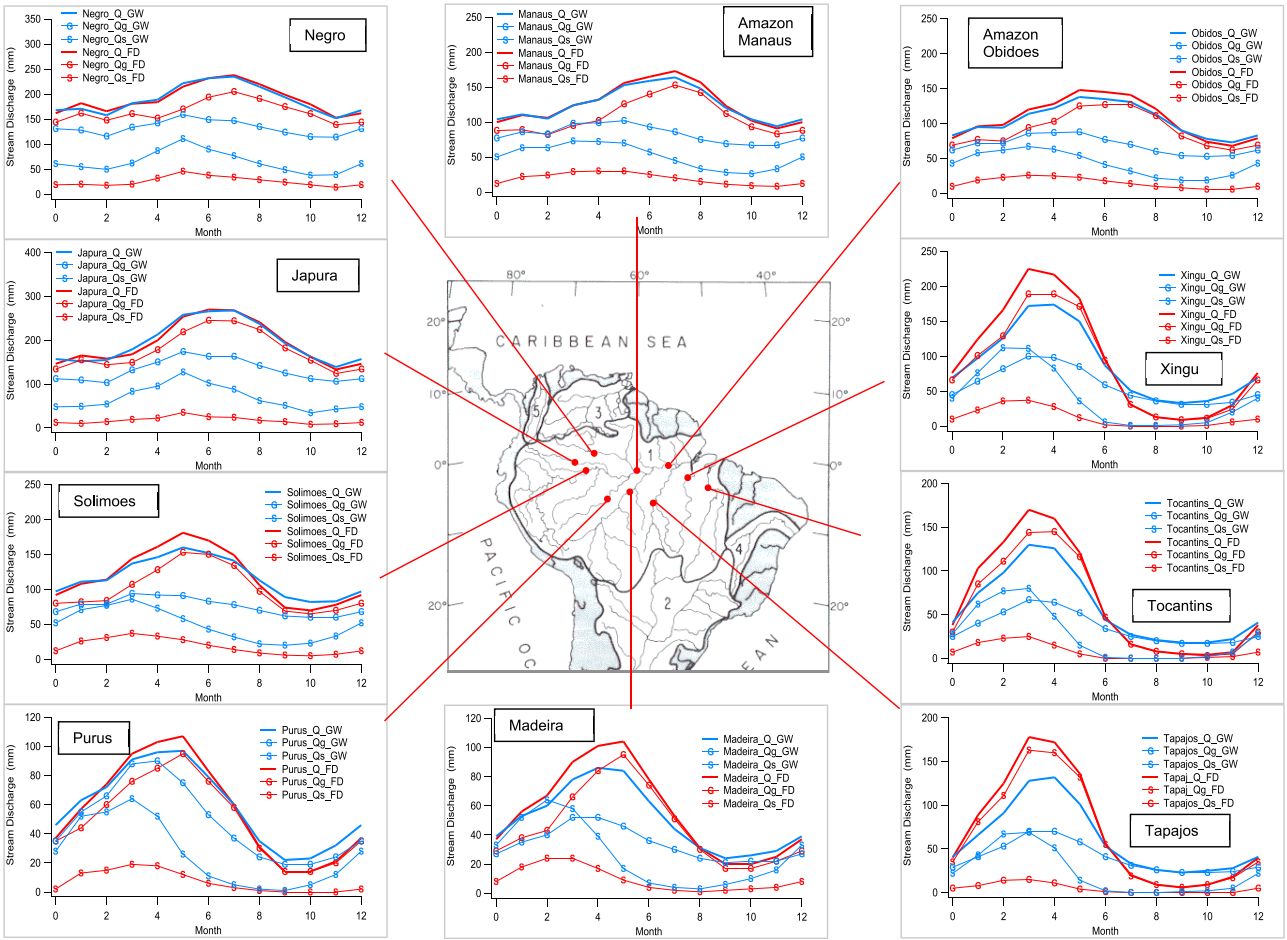

Figure 16. Mean seasonal cycle in streamflow (in mm) with separate contributions from groundwater and surface runoff, for both the GW and FD run.

negligible in northwestern Amazon (Negro and Japura) but significant in the southeastern Amazon. In the northeast, the water table in the GW run is shallower than the 4 m soil column in the FD run, that is, the travel distance through the unsaturated soil zone in the GW run is shorter. This fact, combined with the wetter soil and higher hydraulic conductivity, gives the GW run a much shorter travel time through the unsaturated zone than in the FD run. Although the drainage from the 4 m soil column in the FD run is immediately placed in the rivers, it is compensated by its long travel time through the deep and dry soil column, reducing the difference in river response between the two experiments. In the southeast, the water table is in the range of 10–40 m deep [*Miguez-Macho and Fan*, 2012, Figure 8], far deeper than the 4 m column in the FD run. The long travel distance and the equally dry soil (water table too deep to affect most of the column) cause the travel time in the GW run far longer than in the FD run, delaying the river response.

[90] This brings out the importance of soil water storage as a seasonal buffer for the surface waters. Where the water table is shallow, a fixed, deep soil column may over-estimate the delay of river response to rainfall, and where the water table is deeper, it may under-estimate the delay. Hence a secondary effect of the water table is the altered soil water storage not recognized before.

[91] Regarding the groundwater versus surface runoff contribution to the total discharge, the GW run gives higher surface runoff contributions because of land saturation from below by the rising water table, initiating the 'saturation-excess' runoff (or Dunne runoff), in addition to 'infiltration-excess' runoff (or Horton runoff). In the FD run, the latter is the only surface runoff mechanism. This partition, although having little effect on total river hydrographs, can be important for modeling carbon and nutrient movement from the uplands to the fluvial network as the two hydrologic pathways have different geochemical signatures.

6. Summary, Conclusions and Implications to the Amazon Carbon Cycle

[92] The objective of this study is to evaluate groundwater's influence on the Amazon surface water dynamics using a fully coupled groundwater-surface water model. The simulation is forced with ERA-Interim reanalysis, at 2 km grids and 4 min time steps over 11 yrs (2000–2010). Results are validated with observed streamflow, water table depth and flooding. A parallel run without the groundwater is conducted to reduce the influence of forcing bias. Based on the simulation results, we tested the importance of four mechanisms whereby the groundwater can influence the

surface water features. First, in the headwater catchments across the Amazon, groundwater is the dominant source of streamflow, and its variation from one place to another is a result of varying water table depth. The analyses of 12 headwater catchments across the Amazon indeed highlight the importance of this mechanism. Second, in the floodplains, there are two-way exchanges between the floodwater and groundwater through infiltration in the wet season and seepage in the dry season, but the amount is regulated by the water table depth. The analyses of 5 large floodplains in the Amazon and Orinoco point to the significance of this exchange. Third, groundwater supports wetlands rarely flooded but characterized with a persistently shallow water table, creating water-logged conditions defining wetlands but difficult to observe by remote sensing. Our results suggest that this may occur in the Amazon lowlands and valley floors. Last, the longer time scales of groundwater regulate river flow and surface flooding; because of its delayed and muted response to rainfall, groundwater seeps peak and persist in the dry season, buffering surface waters through seasonal droughts. This point was brought out by the earlier analyses of the 12 headwater catchments and 5 floodplains, and by contrasting the groundwater and free-drain experiments on dry season river discharge. We note that the wet bias in the interim rainfall forcing has led to a similar wet bias in the simulated river discharge, water table depth, valley saturation and induced surface runoff, as well as wetlands, and hence a quantitative conclusion is not reached. Our results here only serve to highlight the mechanisms. A conclusive evaluation of the importance of these mechanisms rests on well-designed field observations that represent the diverse hydrodynamic settings across the Amazon at a range of temporal scales.

[93] Our study may have potential implications to constraining the Amazon carbon cycle. The Amazon ecosystem is thought to be a small sink of atmospheric CO_2 [*Phillips et al.*, 2008] where photosynthetic uptake exceeds loss from terrestrial and aquatic respiration and outgassing to the atmosphere, and fluvial export of dissolved organic, inorganic and particulate carbon to the ocean. All these loss terms are in one way or the other associated with water movement through the landscape; groundwater upwelling and saturation from below suspends and mobilizes soil and litter; the resulting surface runoff washes them into riparian zones and streams; deep soil infiltration dissolves respired CO_2 in soil pores before entering the groundwater, making the latter supersaturated in dissolved CO_2 [*Johnson et al.*, 2008]; groundwater seeps at the headwaters allowing rapid outgassing [*Johnson et al.*, 2006b, 2008; *Davidson et al.*, 2010; *Neu et al.*, 2011], with the seepage area varying seasonally as the water table rises and falls; seasonal inundation of floodplain channels and lakes support aquatic photosynthesis and respiration resulting in additional outgassing [*Richey et al.*, 2002] and fluvial export. A systematic evaluation of the spatial-temporal structures of hydrologic pathways, both above and below the land surface linked by dynamic exchanges, connecting scales from uplands to riparian zones, and from headwater streams to large floodplains, is a necessity for fully constraining the carbon export pathways from the Amazon ecosystem [*Richey et al.*, 2009; 2011].

[94] Methane (CH_4) emission is another carbon escape pathway that is significant in the Amazon [*Bartlett et al.*, 1988; *Devol et al.*, 1990; *Melack et al.*, 2004; *Frankenberg et al.*, 2006; *Bergamaschi et al.*, 2007; *Miller et al.*, 2007; *Belger et al.*, 2011]. Methane emissions have been measured at two end-member scales. At the headwaters, CH_4 evasion from emerging groundwater is found to be significant [*Neu et al.*, 2011]. In the floodplains, CH_4 flux depends on surface inundation and falling of floodwater, which triggers ebullition from shallow sediments [*Engle and Melack*, 2000; *Melack et al.*, 2004; *Belger et al.*, 2011]. Methane is also emitted in wetlands that are never flooded [e.g., *Whalen*, 2005; *Lafleur*, 2008] but with a shallow water table within tens of centimeters of surface. Thus the ability to simulate the Amazon-wide groundwater emergence, the rising and falling of flood waters that are dynamically consistent with the rising and falling of the water table, can support the application of process-based CH_4 flux models [e.g., *Walter and Heimann*, 2000] that can be used to constrain carbon export from the Amazon.

[95] Figure 17 gives some ideas on the likely inter-annual variations in Amazon surface flooding, showing 10 yr (2001–2010) mean flooding frequency (top-left) and the anomaly in each individual years (as number of months each year). The large regional drought in the southwestern Amazon in 2005 and the anomalously wet year of 2009 stand out (but the widely noted 2010 drought is not apparent in the Interim forcing data). Modeling studies such as this may help augment the satellite-based snap shots of Amazon surface water states by providing a dynamic framework with a fine temporal-resolution reconstruction for the past and projections into the future when satellites are not available. An animation is provided as auxiliary material that portrays the inundation of the Amazon over 2001–2005 at 10-day intervals, synchronized with changes in the water table depth.[1] Such coupled evolution among the various hydrologic stores is the norm in nature that needs to be represented in our models. It is our hope that the insights gained here regarding the role of the groundwater reservoir in the Amazon water cycle, together with the integrated modeling tool presented here, can contribute toward quantifying carbon fluxes from the Amazon ecosystem and its role in the global climate.

[96] We end with a discussion of challenges yet to be met by large-scale hydrologic models. Despite our best effort, the model cannot escape from several fundamental deficiencies. One difficulty is with regard to the application of the one-dimensional Richard's equation with fine layers over large model grids of horizontal homogeneity. Our grid size of 2 km cannot differentiate hillslopes from first-order stream valleys, a fundamental scale of water movement on and near the land surface. This topographic gradient from hilltops to valleys also underlies many observed systematic changes in soil and vegetation. Resolving fluxes at this scale over continental regions is crucial but yet infeasible. A second but related difficulty is the use of coarsely gridded global soil maps such as the FAO product, obtained from agricultural surveys of topsoils ($\sim$1 m), for calculating water fluxes in very fine layers. The conversion of the little

[1]Auxiliary materials are available in the HTML. doi:10.1029/2012JD017539.

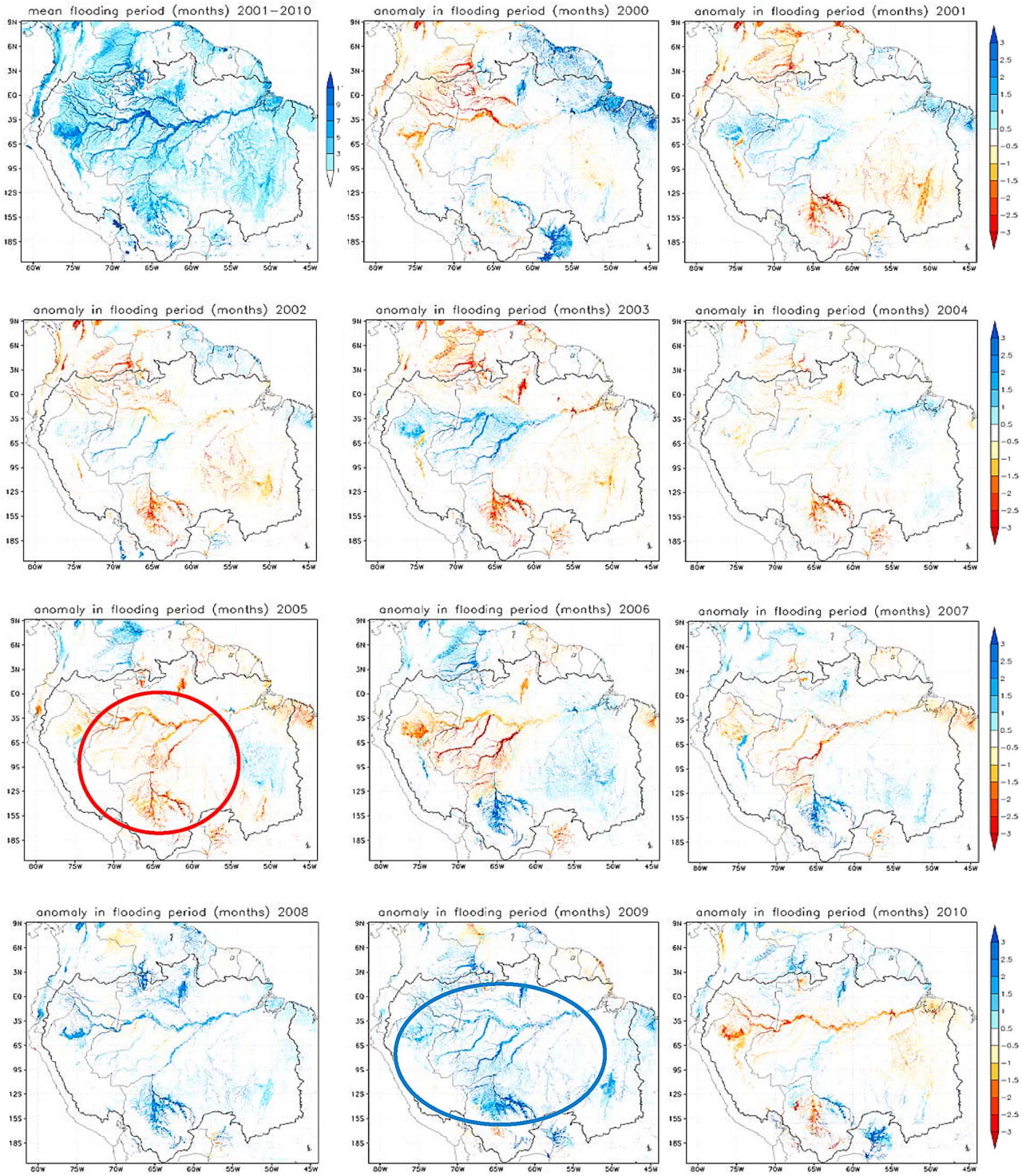

Figure 17. Simulated mean flooding frequency (top-left, as number of months per year) and inter-annual departures, showing the widely reported regional drought of 2005 and the wet year of 2009.

information on soil texture to hydraulic properties, based on a few simple pedo-transfer functions, renders the whole exercise of solving the Richard's equation for centimeter thick model layers rather meaningless. A third (and related to the second) difficulty is the complete lack of information on the hydro-stratigraphy of the subsurface. Groundwater movement is controlled by the permeability structure of sediments and fractured rocks. Despite a century of aquifer characterization in many parts of the world, there remains a complete lack of basic data sets beyond the single-slope or single-aquifer scale, such as the depth to the bedrock and the vertical structures of porosity and permeability. Large-scale

land models must rely on assumptions such as exponential decay of permeability with depth, which is widely adopted but at the same time widely known to grossly misrepresent the real-world. These difficulties can only be addressed collectively and in time. The saving grace is that the land surface topography has an enormous power in driving the movement of water at and near the surface. As shown here, by simply allowing the gravity-driven flow in the subsurface, and letting the water level difference to determine the groundwater-surface water exchange, one can gain important, albeit qualitative, insights on the likely hydrologic states and fluxes near the land surface.

[97] **Acknowledgments.** Financial support comes from Ministerio de Educación y Ciencia de España (Spanish Ministry of Education and Science) CGL2006–13828, NSF-AGS-1045110, and EPA-STAR-RD834190. Computational support is provided by CESGA (Centro de Supercomputación de Galicia) Supercomputer Center at the Universidade de Santiago de Compostela, Galicia, Spain. We thank Dai Yamazaki for helpful discussions on solving the diffusive wave equation at large scales, and John Melack for directing us to the LBA flooding data. Finally we thank the two anonymous referees for their insightful and in-depth reviewers and the many constructive comments.

References

Aalto, R., L. Maurice-Bourgoin, T. Dunne, D. R. Montgomery, C. A. Nittrouer, and J. L. Guyot (2003), Episodic sediment accumulation on Amazon floodplains influenced by El Nino/Southern Oscillation, *Nature*, *425*, 493–497, doi:10.1038/nature02002.

Adler, R. F., et al. (2003), The version 2 Global Precipitation Climatology Project (GPCP) monthly precipitation analysis (1979–present), *J. Hydrometeorol.*, *4*, 1147–1167, doi:10.1175/1525-7541(2003)004<1147:TVGPCP>2.0.CO;2.

Ahnert, F. (1970), Functional relationships between denudation, relief, and uplift in large mid-latitude drainage basins, *Am. J. Sci.*, *268*, 243–263, doi:10.2475/ajs.268.3.243.

Alkama, R., B. R. Decharme, H. Douville, M. Becker, A. Cazenave, J. Sheffield, A. Voldoire, S. Tyteca, and P. Le Moigne (2010), Global evaluation of the ISBA-TRIP continental hydrological system. Part I: Comparison with GRACE terrestrial water storage estimates and in situ river discharges, *J. Hydrometeorol.*, *11*, 583–600, doi:10.1175/2010JHM1211.1.

Alsdorf, D., P. Bates, J. Melack, M. Wilson, and T. Dunne (2007), Spatial and temporal complexity of the Amazon flood measured from space, *Geophys. Res. Lett.*, *34*, L08402, doi:10.1029/2007GL029447.

Anyah, R., C. P. Weaver, G. Miguez-Macho, Y. Fan, and A. Robock (2008), Incorporating water table dynamics in climate modeling: 3. Simulated groundwater influence on coupled land-atmosphere variability, *J. Geophys. Res.*, *113*, D07103, doi:10.1029/2007JD009087.

Balsamo, G., P. Viterbo, A. Beljaars, B. van den Hurk, M. Hirschi, A. K. Betts, and K. Scipal (2009), A revised hydrology for the ECMWF model: Verification from field site to terrestrial water storage and impact in the Integrated Forecast System, *J. Hydrometeorol.*, *10*, 623–643, doi:10.1175/2008JHM1068.1.

Bartlett, K., P. Crill, D. Sebacher, R. Harriss, J. Wilson, and J. Melack (1988), Methane flux from the central Amazonian floodplain, *J. Geophys. Res.*, *93*, 1571–1582, doi:10.1029/JD093iD02p01571.

Bates, P. D., M. S. Horritt, and T. J. Fewtrell (2010), A simple inertial formulation of the shallow water equations for efficient two-dimensional flood inundation modeling, *J. Hydrol.*, *387*, 33–45, doi:10.1016/j.jhydrol.2010.03.027.

Bauer, P., T. Gumbricht, and W. Kinzelbach (2006), A regional coupled surface water/groundwater model of the Okavango Delta, Botswana, *Water Resour. Res.*, *42*, W04403, doi:10.1029/2005WR004234.

Beighley, R. E., K. G. Eggert, T. Dunne, Y. He, V. Gummadi, and K. L. Verdin (2009), Simulating hydrologic and hydraulic processes throughout the Amazon River Basin, *Hydrol. Processes*, *23*, 1221–1235, doi:10.1002/hyp.7252.

Belger, L., B. R. Forsberg, and J. M. Melack (2011), Carbon dioxide and methane emissions from interfluvial wetlands in the upper Negro River basin, Brazil, *Biogeochemistry*, *105*, 171–183, doi:10.1007/s10533-010-9536-0.

Bergamaschi, P., et al. (2007), Satellite chartography of atmospheric methane from SCIAMACHY onboard ENVISAT: 2. Evaluation based on inverse model simulations, *J. Geophys. Res.*, *112*, D02304, doi:10.1029/2006JD007268.

Betson, R. P., and J. B. Marius (1969), Source area of storm runoff, *Water Resour. Res.*, *5*(3), 574–582, doi:10.1029/WR005i003p00574.

Betts, A. K., M. Kohler, and Y. Zhang (2009), Comparison of river basin hydrometeorology in ERA-Interim and ERA-40 reanalyses with observations, *J. Geophys. Res.*, *114*, D02101, doi:10.1029/2008JD010761.

Beven, K. J., and M. J. Kirkby (1979), A physically based, variable contributing area model of basin hydrology, *Hydrol. Sci. Bull.*, *24*, 43–69, doi:10.1080/02626667909491834.

Bierkens, M. F. P., and B. J. J. M. van den Hurk (2007), Groundwater convergence as a possible mechanism for multi-year persistence in rainfall, *Geophys. Res. Lett.*, *34*, L02402, doi:10.1029/2006GL028396.

Bongers, F., D. Engelen, and H. Klinge (1985), Phytomass structure of natural plant communities on spodosols in southern Venezuela: The Bana woodland, *Vegetatio*, *63*, 13–34, doi:10.1007/BF00032183.

Bonnet, M. P., et al. (2008), Floodplain hydrology in an Amazon floodplain lake (Lago Grande de Curuaı), *J. Hydrol.*, *349*, 18–30, doi:10.1016/j.jhydrol.2007.10.055.

Borma, L. S., et al. (2009), Atmosphere and hydrologic controls of the evapotranspiration over a floodplain forest in the Bananal Island region, Amazonia, *J. Geophys. Res.*, *114*, G01003, doi:10.1029/2007JG000641.

Bourrel, L., L. Phillips, and S. Moreau (2009), The dynamics of floods in the Bolivian Amazon Basin, *Hydrol. Processes*, *23*, 3161–3167, doi:10.1002/hyp.7384.

Carabajal, C. C., and D. J. Harding (2006), SRTM C-band and ICESat laser altimetry elevation comparisons as a function of tree cover and relief, *Photogramm. Eng. Remote Sens.*, *72*, 287–298.

Carmo, J. B., M. Keller, J. D. Dias, P. B. Camargo, and P. Crill (2006), A source of methane from upland forests in the Brazilian Amazon, *Geophys. Res. Lett.*, *33*, L04809, doi:10.1029/2005GL025436.

Chapelon, N., H. Douville, P. Kosuth, and T. Oki (2002), Off-line simulation of the Amazon water balance: A sensitivity study with implications for GSWP, *Clim. Dyn.*, *19*, 141–154.

Choi, H. I., and X.-Z. Liang (2010), Improved terrestrial hydrologic representation in mesoscale land surface models, *J. Hydrometeorol.*, *11*, 797–809, doi:10.1175/2010JHM1221.1.

Clapp, R. B., and G. M. Hornberger (1978), Empirical equations for some soil hydraulic properties, *Water Resour. Res.*, *14*, 601–604, doi:10.1029/WR014i004p00601.

Clapperton, C. (1993), *Quaternary Geology and Geomorphology of South America*, Elsevier, Amsterdam.

Coe, M. T., M. H. Costa, A. Botta, and C. M. Birkett (2002), Long-term simulations of discharge and floods in the Amazon Basin, *J. Geophys. Res.*, *107*(D20), 8044, doi:10.1029/2001JD000740.

Coe, M. T., M. H. Costa, and E. A. Howard (2008), Simulating the surface waters of the Amazon River basin: Impacts of new river geomorphic and flow parameterizations, *Hydrol. Processes*, *22*, 2542–2553, doi:10.1002/hyp.6850.

Coomes, D. A., and P. J. Grubb (1996), Amazonian caatinga and related communities at La Esmeralda, Venezuela: Forest structure, physiognomy and floristics, and control by soil factors, *Vegetatio*, *122*, 167–191, doi:10.1007/BF00044699.

Costa, M. H., and J. A. Foley (1997), Water balance of the Amazon Basin: Dependence on vegetation cover and canopy conductance, *J. Geophys. Res.*, *102*(D20), 23,973–23,989, doi:10.1029/97JD01865.

Cuartas, L. A. (2008), Estudo Observacional E De Modelagem Hidrologica De Uma Micro-Bacia Em Floresta Nao Perturbada Na Amazonia Central, PhD thesis, Inst. Nac. de Pesqui. Espaciais, Sao Jose dos Campos, Brazil.

Cullmann, J., W. J. Junk, G. Weber, and G. H. Schmitz (2006), The impact of seepage influx on cation content of a Central Amazonian floodplain lake, *J. Hydrol.*, *328*, 297–305, doi:10.1016/j.jhydrol.2005.12.027.

Davidson, E. A., R. O. Figueiredo, D. Markewitz, and A. K. Aufdenkampe (2010), Dissolved CO_2 in small catchment streams of eastern Amazonia: A minor pathway of terrestrial carbon loss, *J. Geophys. Res.*, *115*, G04005, doi:10.1029/2009JG001202.

Decharme, B., H. Douville, C. Prigent, F. Papa, and F. Aires (2008), A new river flooding scheme for global climate applications: Off-line evaluation over South America, *J. Geophys. Res.*, *113*, D11110, doi:10.1029/2007JD009376.

Decharme, B., R. Alkama, H. Douville, M. Becker, and A. Cazenave (2010), Global evaluation of the ISBA-TRIP continental hydrological system. Part II: Uncertainties in river routing simulation related to flow velocity and groundwater storage, *J. Hydrometeorol.*, *11*, 601–617, doi:10.1175/2010JHM1212.1.

Dee, D. P., et al. (2011), The ERA-Interim reanalysis: Configuration and performance of the data assimilation system, *Q. J. R. Meteorol. Soc.*, *137*, 553–597, doi:10.1002/qj.828.

Devol, A. H., J. E. Richey, B. R. Forsberg, and L. A. Martinelli (1990), Seasonal dynamics in methane emissions from the Amazon River floodplain to the troposphere, *J. Geophys. Res.*, *95*(D10), 16,417–16,426.

de Vries, J. J. (1994), Dynamics of the interface between streams and groundwater systems in lowland areas, with reference to stream net evolution, *J. Hydrol.*, *155*, 39–56, doi:10.1016/0022-1694(94)90157-0.

de Vries, J. J. (1995), Seasonal expansion and contraction of stream networks in shallow groundwater system, *J. Hydrol.*, *170*, 15–26, doi:10.1016/0022-1694(95)02684-H.

Do Nascimento, N. R., E. Fritsch, G. T. Bueno, M. Bardy, C. Grimaldi, and A. J. Melfi (2008), Podzolization as a deferralitization process: Dynamics and chemistry of ground and surface waters in an Acrisol–Podzol sequence of the upper Amazon Basin, *Eur. J. Soil Sci.*, *59*, 911–924, doi:10.1111/j.1365-2389.2008.01049.x.

Dunne, T., and R. D. Black (1970a), An experimental investigation of runoff production in permeable soils, *Water Resour. Res.*, *6*(2), 478–490, doi:10.1029/WR006i002p00478.

Dunne, T., and R. D. Black (1970b), Partial area contributions to storm runoff in a small New England watershed, *Water Resour. Res.*, *6*, 1296–1311, doi:10.1029/WR006i005p01296.

Dunne, T., and L. A. K. Mertes (2007), Rivers, in *The Physical Geography of South America*, edited by T. T. Veblen, K. R. Young, and A. R. Orme, chap. 5, pp. 76–90, Oxford Univ. Press, Oxford, U. K.

Dunne, T., L. A. K. Mertes, R. H. Meade, J. E. Richey, and B. R. Forsberg (1998), Exchanges of sediment between the flood plain and channel of the Amazon River in Brazil, *Geol. Soc. Am. Bull.*, *110*(4), 450–467, doi:10.1130/0016-7606(1998)110<0450:EOSBTF>2.3.CO;2.

Eltahir, E., and P. J.-F. Yeh (1999), On the asymmetric response of aquifer water level to floods and droughts in Illinois, *Water Resour. Res.*, *35*, 1199–1217, doi:10.1029/1998WR900071.

Engle, D., and J. M. Melack (2000), Methane emissions from an Amazon floodplain lake: Enhanced release during episodic mixing and during falling water, *Biogeochemistry*, *51*, 71–90, doi:10.1023/A:1006389124823.

Eva, H. D., et al. (2002), A vegetation map of South America, Eur. Comm. Joint Res. Cent., Brussels. [Available at http://bioval.jrc.ec.europa.eu/products/glc2000/products.php.]

Eva, H. D., A. S. Belward, E. E. de Miranda, C. M. di Bella, V. Gonds, O. Huber, S. Jones, M. Sgrenzaroli, and S. Fritz (2004), A land cover map of South America, *Global Change Biol.*, *10*, 1–14, doi:10.1111/j.1529-8817.2003.00774.x.

Fan, Y., and G. Miguez-Macho (2010), Potential groundwater contribution to Amazon dry-season evapotranspiration, *Hydrol. Earth Syst. Sci.*, *14*, 2039–2056, doi:10.5194/hess-14-2039-2010.

Fan, Y., and G. Miguez-Macho (2011), A simple hydrologic framework for simulating wetlands in climate and earth system models, *Clim. Dyn.*, *37*(1–2), 253–278, doi:10.1007/s00382-010-0829-8.

Fan, Y., G. Miguez-Macho, C. P. Weaver, R. Walko, and A. Robock (2007), Incorporating water table dynamics in climate modeling: 1. Water table observations and the equilibrium water table, *J. Geophys. Res.*, *112*, D10125, doi:10.1029/2006JD008111.

Ferguson, I. M., and R. M. Maxwell (2010), Role of groundwater in watershed response and land surface feedbacks under climate change, *Water Resour. Res.*, *46*, W00F02, doi:10.1029/2009WR008616.

Foley, J. A., A. Botta, M. T. Coe, and M. H. Costa (2002), El Nino–Southern oscillation and the climate, ecosystems and rivers of Amazonia, *Global Biogeochem. Cycles*, *16*(4), 1132, doi:10.1029/2002GB001872.

Forsberg, B. R., A. H. Devol, J. E. Richey, L. A. Martinelli, and H. dos Sandos (1988), Factors controlling nutrient concentrations in Amazon floodplain lakes, *Limnol. Oceanogr.*, *33*, 41–56, doi:10.4319/lo.1988.33.1.0041.

Frankenberg, C., J. F. Meirink, P. Bergamaschi, A. P. H. Goede, M. Heimann, S. Ko¨rner, U. Platt, M. van Weele, and T. Wagner (2006), Satellite chartography of atmospheric methane from SCIAMACHYon board ENVISAT: Analysis of the years 2003 and 2004, *J. Geophys. Res.*, *111*, D07303, doi:10.1029/2005JD006235.

Freeze, R. A. (1971), Three-dimensional, transient, saturated-unsaturated flow in a groundwater basin, *Water Resour. Res.*, *7*(2), 347–366, doi:10.1029/WR007i002p00347.

Freeze, R. A., and J. A. Cherry (1979), *Groundwater*, 604 pp., Prentice Hall, Upper Saddle River, N. J.

Germer, S., C. Neill, A. V. Krusche, and H. Elsenbeer (2010), Influence of land-use change on near-surface hydrological processes: Undisturbed forest to pasture, *J. Hydrol.*, *380*, 473–480, doi:10.1016/j.jhydrol.2009.11.022.

Grogan, J., and J. Galvão (2006), Physiographic and floristic gradients across topography in transitional seasonally dry evergreen forests of southeast Para, Brazil, *Acta Amazon.*, *36*, 483–496, doi:10.1590/S0044-59672006000400009.

Gulden, L. E., E. Rosero, Z.-L. Yang, M. Rodell, C. S. Jackson, G. Y. Niu, P. J.-F. Yeh, and J. Famiglietti (2007), Improving land-surface model hydrology: Is an explicit aquifer model better than a deeper soil profile?, *Geophys. Res. Lett.*, *34*, L09402, doi:10.1029/2007GL029804.

Gutowski, W. J., Jr., C. J. Vorosmarty, M. Person, Z. Otles, B. Fekete, and J. York (2002), A Coupled Land-Atmosphere Simulation Program (CLASP): Calibration and validation, *J. Geophys. Res.*, *107*(D16), 4283, doi:10.1029/2001JD000392.

Hamilton, S. K., J. Kellndorfer, B. Lehner, and M. Tobler (2007), Remote sensing of floodplain geomorphology as a surrogate for biodiversity in a tropical river system (Madre de Dios, Peru), *Geomorphology*, *89*, 23–38, doi:10.1016/j.geomorph.2006.07.024.

Harbaugh, A. W., E. R. Banta, M. C. Hill, and M. G. McDonald (2000), Modflow-2000, the U.S. Geological Survey modular groundwater model - User guide to modularization concepts and the groundwater flow process, *U.S. Geol. Surv. Open File Rep.*, *00-92*, 130 pp.

Heimsath, A. M., W. E. Dietrich, K. Nishiizumi, and R. C. Finkel (1997), The soil production function and landscape equilibrium, *Nature*, *388*, 358–361, doi:10.1038/41056.

Hess, L. L., J. M. Melack, E. M. L. M. Novo, C. C. F. Barbosa, and M. Gastil (2003), Dual-season mapping of wetland inundation and vegetation for the central Amazon basin, *Remote Sens. Environ.*, *87*, 404–428, doi:10.1016/j.rse.2003.04.001.

Hess, L. L., J. M. Melack, E. M. L. M. Novo, C. C. F. Barbosa, and M. Gastil (2009), LBA-ECO LC-07 Central Amazon Wetlands 100 m Mask based on JERS SAR Images (v.0), http://www.daac.ornl.gov, Oak Ridge Natl. Lab., Oak Ridge, Tenn.

Hewlett, J. D., and A. R. Hibbert (1963), Moisture and energy conditions with a sloping soil mass during drainage, *J. Geophys. Res.*, *68*, 1081–1087, doi:10.1029/JZ068i004p01081.

Hodnett, M. G., I. Vendrame, O. De, A. Marques Filho, M. D. Oyama, and J. Tomasella (1997a), Soil water storage and groundwater behaviour in a catenary sequence beneath forest in central Amazonia: I. Comparisons between plateau, slope and valley floor, *Hydrol. Earth Syst. Sci.*, *1*, 265–277, doi:10.5194/hess-1-265-1997.

Hodnett, M. G., I. Vendrame, O. De, A. Marques Filho, M. D. Oyama, and J. Tomasella (1997b), Soil water storage and groundwater behaviour in a catenary sequence beneath forest in central Amazonia. II. Floodplain water table behaviour and implications for streamflow generation, *Hydrol. Earth Syst. Sci.*, *1*, 279–290, doi:10.5194/hess-1-279-1997.

Hooke, R. L. (2000), Toward a uniform theory of clastic sediment yield in fluvial systems, *Geol. Soc. Am. Bull.*, *112*, 1778–1786, doi:10.1130/0016-7606(2000)112<1778:TAUTOC>2.0.CO;2.

Hunter, N. M., P. D. Bates, M. S. Horritt, and M. D. Wilson (2007), Simple spatially distributed models for predicting flood inundation: A review, *Geomorphology*, *90*, 208–225, doi:10.1016/j.geomorph.2006.10.021.

Jiang, X. Y., G. Y. Niu, and Z. L. Yang (2009), Impacts of vegetation and groundwater dynamics on warm season precipitation over the Central United States, *J. Geophys. Res.*, *114*, D06109, doi:10.1029/2008JD010756.

Jirka, S., A. J. McDonald, M. S. Johnson, T. R. Feldpausch, E. G. Couto, and S. J. Riha (2007), Relationships between soil hydrology and forest structure and composition in the southern Brazilian Amazon, *J. Veg. Sci.*, *18*, 183–194, doi:10.1111/j.1654-1103.2007.tb02529.x.

Johnson, M. S., et al. (2006a), Organic carbon fluxes within and streamwater exports from headwater catchments in the southern Amazon, *Hydrol. Processes*, *20*, 2599–2614, doi:10.1002/hyp.6218.

Johnson, M. S., J. Lehmann, E. G. Couto, J. P. N. Filho, and S. J. Riha (2006b), DOC and DIC in flowpaths of Amazonian headwater catchments with hydrologically contrasting soils, *Biogeochemistry*, *81*(1), 45–57, doi:10.1007/s10533-006-9029-3.

Johnson, M. S., J. Lehmann, S. J. Riha, A. V. Krusche, J. E. Richey, J. P. H. B. Ometto, and E. G. Couto (2008), CO_2 efflux from Amazonian headwater streams represents a significant fate for deep soil respiration, *Geophys. Res. Lett.*, *35*, L17401, doi:10.1029/2008GL034619.

Juárez, R. I. N., W. H. Li, R. Fu, K. Fernandes, and A. D. Cardoso (2009), Comparison of precipitation datasets over the tropical South American and African continents, *J. Hydrometeorol.*, *10*(1), 289–299, doi:10.1175/2008JHM1023.1.

Kalliola, R., M. Puhakka, J. Salo, H. Tuomisto, and K. Ruokolainen (1991), The dynamics, distribution and classification of swamp vegetation in Peruvian Amazonia, *Ann. Bot. Fenn.*, *28*, 225–239.

Kalliola, R., J. Salo, M. Puhakka, M. Rajasilta, T. Häme, R. J. Neller, M. E. Räsänen, and W. A. Danjoy Arias (1992), Upper Amazon channel migration, *Naturwissenschaften*, *79*, 75–79, doi:10.1007/BF01131806.

Kollet, S. J., and R. M. Maxwell (2006), Integrated surface-groundwater flow modeling: A free-surface overland flow boundary condition in a parallel groundwater flow model, *Adv. Water Resour.*, *29*(7), 945–958, doi:10.1016/j.advwatres.2005.08.006.

Lafleur, P. M. (2008), Connecting atmosphere and wetland: Energy and water vapour exchange, *Geogr. Compass*, *2*, 1027–1057, doi:10.1111/j.1749-8198.2007.00132.x.

Lähteenoja, O., and S. Page (2011), High diversity of tropical peatland ecosystem types in the Pastaza-Marañón basin, Peruvian Amazonia, *J. Geophys. Res.*, *116*, G02025, doi:10.1029/2010JG001508.

Lam, A., D. Karssenberg, B. J. J. M. van den Hurk, and M. F. P. Bierkens (2011), Spatial and temporal connections in groundwater contribution to evaporation, *Hydrol. Earth Syst. Sci.*, *15*, 2621–2630, doi:10.5194/hess-15-2621-2011.

Latrubesse, E. M., J. C. Stevaux, and R. Sinha (2005), Tropical rivers, *Geomorphology*, *70*, 187–206, doi:10.1016/j.geomorph.2005.02.005.

Leopold, L. B., and T. Maddock (1953), The hydraulic geometry of stream channels and some physiographic implications, *U.S. Geol. Surv. Prof. Pap.*, *252*, 55 pp.

Leopoldo, P. R., W. K. Franken, and N. A. Villa Nova (1995), Real evapotranspiration and transpiration through a tropical rain forest in central Amazonia as estimated by the water balance method, *For. Ecol. Manage.*, *73*, 185–195, doi:10.1016/0378-1127(94)03487-H.

Lesack, L. F. W. (1993), Water balance and hydrologic characteristics of a rain forest catchment in the central Amazon Basin, *Water Resour. Res.*, *29*, 759–773, doi:10.1029/92WR02371.

Lesack, L. F. W. (1995), Seepage exchange in an Amazon floodplain lake, *Limnol. Oceanogr.*, *40*, 598–609, doi:10.4319/lo.1995.40.3.0598.

Lesack, L. F. W., and J. M. Melack (1995), Flooding hydrology and mixture dynamics of lake water derived from multiple sources in an Amazon floodplain lake, *Water Resour. Res.*, *31*, 329–345, doi:10.1029/94WR02271.

Liang, X., Z. Xie, and M. Huang (2003), A new parameterization for surface and ground water interactions and its impact on water budgets with the Variable Infiltration Capacity (VIC) landsurface model, *J. Geophys. Res.*, *108*(D16), 8613, doi:10.1029/2002JD003090.

Lo, M.-H., and J. S. Famiglietti (2010), Effect of water table dynamics on land surface hydrologic memory, *J. Geophys. Res.*, *115*, D22118, doi:10.1029/2010JD014191.

Lo, M.-H., and J. S. Famiglietti (2011), Precipitation response to land subsurface hydrologic processes in atmospheric general circulation model simulations, *J. Geophys. Res.*, *116*, D05107, doi:10.1029/2010JD015134.

Lo, M.-H., P. J. F. Yeh, and J. S. Famiglietti (2008), Constraining water table depth simulations in a land surface model using estimated baseflow, *Adv. Water Resour.*, *31*(12), 1552–1564, doi:10.1016/j.advwatres.2008.06.007.

Lo, M.-H., J. S. Famiglietti, P. J. F. Yeh, and T. H. Syed (2010), Improving parameter estimation and water table depth simulation in a land surface model using GRACE water storage and estimated base flow data, *Water Resour. Res.*, *46*, W05517, doi:10.1029/2009WR007855.

Manning, C. E., and S. E. Ingebritsen (1999), Permeability of the continental crust: Implications of geothermal data and metamorphic systems, *Rev. Geophys.*, *37*, 127–150, doi:10.1029/1998RG900002.

Marani, M., E. Eltahir, and A. Rinaldo (2001), Geomorphic controls on regional base flow, *Water Resour. Res.*, *37*, 2619–2630, doi:10.1029/2000WR000119.

Maxwell, R. M., and S. J. Kollet (2008), Interdependence of groundwater dynamics and land-energy feedbacks under climate change, *Nat. Geosci.*, *1*, 665–669, doi:10.1038/ngeo315.

Maxwell, R. M., and N. L. Miller (2005), Development of a coupled land surface and groundwater model, *J. Hydrometeorol.*, *6*, 233–247, doi:10.1175/JHM422.1.

McCarthy, T. S. (2006), Groundwater in the wetlands of the Okavango Delta, Botswana, and its contribution to the structure and function of the ecosystem, *J. Hydrol.*, *320*, 264–282, doi:10.1016/j.jhydrol.2005.07.045.

McClain, M. E., J. E. Richey, and J. A. Brandes (1997), Dissolved organic matter and terrestrial-lotic linkages in the central Amazon basin of Brazil, *Global Biogeochem. Cycles*, *11*, 295–311, doi:10.1029/97GB01056.

Meade, R. H., J. M. Rayol, S. C. da Conceicao, and J. R. G. Natividate (1991), Backwater effects in the Amazon River Basin of Brazil, *Environ. Geol. Water Sci.*, *18*(2), 105–114, doi:10.1007/BF01704664.

Melack, J. M., and L. L. Hess (2011), Remote sensing of the distribution and extent of wetlands in the Amazon basin, *Ecol. Stud.*, *210*, 43–59, doi:10.1007/978-90-481-8725-6_3.

Melack, J. M., L. L. Hess, M. Gastil, B. R. Forsberg, S. K. Hamilton, I. B. T. Lima, and E. Novo (2004), Regionalization of methane emissions in the Amazon basin with microwave remote sensing, *Global Change Biol.*, *10*(5), 530–544, doi:10.1111/j.1365-2486.2004.00763.x.

Mertes, L. A. K. (1997), Documentation and significance of the perirheic zone on inundated floodplains, *Water Resour. Res.*, *33*, 1749–1762, doi:10.1029/97WR00658.

Mertes, L. A. K., T. Dunne, and L. A. Martinelli (1996), Channel-floodplain geomorphology along the Solimmoes-Amazon River, Brazil, *Geol. Soc. Am. Bull.*, *108*(9), 1089–1107, doi:10.1130/0016-7606(1996)108<1089:CFGATS>2.3.CO;2.

Miguez-Macho, G., and Y. Fan (2012), The role of groundwater in the Amazon water cycle: 2. Influence on seasonal soil moisture and evapotranspiration, *J. Geophys. Res.*, *117*, D15114, doi:10.1029/2012JD017540.

Miguez-Macho, G., Y. Fan, C. P. Weaver, R. Walko, and A. Robock (2007), Incorporating water table dynamics in climate modeling: 2. Formulation, validation, and soil moisture simulation, *J. Geophys. Res.*, *112*, D13108, doi:10.1029/2006JD008112.

Miguez-Macho, G., H. Li, and Y. Fan (2008), Simulated water table and soil moisture climatology over North America: Does the water table matter?, *Bull. Am. Meteorol. Soc.*, *89*(5), 663–672, doi:10.1175/BAMS-89-5-663.

Miller, J. B., L. V. Gatti, M. T. S. d'Amelio, A. M. Crotwell, E. J. Dlugokencky, P. Bakwin, P. Artaxo, and P. P. Tans (2007), Airborne measurements indicate large methane emissions from the eastern Amazon basin, *Geophys. Res. Lett.*, *34*, L10809, doi:10.1029/2006GL029213.

Mohamed, Y. A., H. H. G. Savenije, W. G. M. Bastiaanssen, and B. J. J. M. van den Hurk (2006), New lessons on the Sudd hydrology learned from remote sensing and climate modeling, *Hydrol. Earth Syst. Sci.*, *10*, 507–518, doi:10.5194/hess-10-507-2006.

Nepstad, D. C., et al. (2002), The effects of partial throughfall exclusion on canopy processes, aboveground production, and biogeochemistry of an Amazon forest, *J. Geophys. Res.*, *107*(D20), 8085, doi:10.1029/2001JD000360.

Neu, V., C. Neill, and A. V. Krusche (2011), Gaseous and fluvial carbon export from an Amazon forest watershed, *Biogeochemistry*, *105*, 133–147, doi:10.1007/s10533-011-9581-3.

Niu, G.-Y., Z. L. Yang, R. E. Dickinson, L. E. Gulden, and H. Su (2007), Development of a simple groundwater model for use in climate models and evaluation with Gravity Recovery and Climate Experiment data, *J. Geophys. Res.*, *112*, D07103, doi:10.1029/2006JD007522.

Niu, G.-Y., et al. (2011), The community Noah land surface model with multiparameterization options (Noah-MP): 1. Model description and evaluation with local-scale measurements, *J. Geophys. Res.*, *116*, D12109, doi:10.1029/2010JD015139.

Oleson, K. W. et al. (2010) Technical description of version 4.0 of the Community Land Model (CLM), *NCAR/TN-478+STR*, Natl. Cent. for Atmos. Res., Boulder, Colo.

Papa, F., C. Prigent, F. Aires, C. Jimenez, W. B. Rossow, and E. Matthews (2010), Interannual variability of surface water extent at the global scale, 1993–2004, *J. Geophys. Res.*, *115*, D12111, doi:10.1029/2009JD012674.

Pelletier, J. D., and C. Rasmussen (2009), Geomorphically based predictive mapping of soil thickness in upland watersheds, *Water Resour. Res.*, *45*, W09417, doi:10.1029/2008WR007319.

Phillips, O. L., S. L. Lewis, T. R. Baker, K.-J. Chao, and N. Higuchi (2008), The changing Amazon forest, *Philos. Trans. R. Soc. B*, *363*, 1819–1827, doi:10.1098/rstb.2007.0033.

Poels, R. L. H. (1987), *Soils, Water and Nutrients in a Forest Ecosystem in Suriname*, Agric. Univ. at Wageningen, Wageningen, Netherlands.

Prance, G. T. (1987), Soils and vegetation, in *Biogeography and Quaternary History in Tropical America*, edited by T. C. Whitmore and G. T. Prance, pp. 19–45, Clarendon Press, Oxford, U. K.

Press, W. H., B. P. Flannery, S. A. Teukolsky, and W. T. Vetterling (1989), *Numerical Recipes–The Art of Scientific Computing (FORTRAN Version)*, 702 pp., Cambridge Univ. Press, Cambridge, U. K.

Prigent, C., F. Papa, F. Aires, W. B. Rossow, and E. Matthews (2007), Global inundation dynamics inferred from multiple satellite observations, 1993–2000, *J. Geophys. Res.*, *112*, D12107, doi:10.1029/2006JD007847.

Räsänen, M. E., J. S. Salo, H. Jungner, and L. Romero Pittman (1990), Evolution of the western Amazon lowland relief: Impact of Andean foreland dynamics, *Terra Nova*, *2*, 320–332.

Räsänen, M., R. Neller, J. Salo, and H. Jungner (1992), Recent and ancient fluvial deposition systems in the Amazonian foreland basin, Peru, *Geol. Mag.*, *129*, 293–306, doi:10.1017/S0016756800019233.

Richey, J. E., C. Nobre, and C. Desser (1989a), Amazon River discharge and climate variability: 1903 to 1985, *Science*, *246*, 101–103, doi:10.1126/science.246.4926.101.

Richey, J. E., L. A. K. Mertes, T. Dunne, R. L. Victoria, B. R. Forsberg, A. C. N. S. Tancredi, and E. Oliveira (1989b), Sources and routing of the Amazon River flood wave, *Global Biogeochem. Cycles*, *3*, 191–204, doi:10.1029/GB003i003p00191.

Richey, J. E., J. M. Melack, A. K. Aufdenkampe, V. M. Ballester, and L. L. Hess (2002), Outgassing from Amazonian rivers and wetlands as a large tropical source of atmospheric CO2, *Nature*, *416*, 617–620, doi:10.1038/416617a.

Richey, J. E., A. V. Krusche, M. S. Johnson, H. B. da Cunha, and M. V. Ballester (2009), The role of rivers in the regional carbon balance, in *Amazonia and Global Change*, *Geophys. Monogr. Ser.*, vol. 186, edited by M. Keller et al., pp. 489–504, AGU, Washington, D. C., doi:10.1029/2008GM000734.

Richey, J. E., M. V. Ballester, E. A. Davidson, M. S. Johnson, and A. Krusche (2011), Land-Water interactions in the Amazon, *Biogeochemistry*, *105*, 1–5, doi:10.1007/s10533-011-9622-y.

Rihani, J. F., R. M. Mazwell, and F. K. Chow (2010), Coupling groundwater and land surface processes: Idealized simulations to identify effects of

terrain and subsurface heterogeneity on land surface energy fluxes, *Water Resour. Res.*, *46*, W12523, doi:10.1029/2010WR009111.

Rodell, M., et al. (2004), The global land data assimilation system, *Bull. Am. Meteorol. Soc.*, *85*, 381–394, doi:10.1175/BAMS-85-3-381.

Rojstaczer, S. A., S. E. Ingebritsen, and D. O. Hayba (2008), Permeability of continental crust influenced by internal and external forcing, *Geofluids*, *8*, 128–139, doi:10.1111/j.1468-8123.2008.00211.x.

Romero-Saltos, H. L., L. S. L. Sternberg, M. Z. Moreira, and D. C. Nepstad (2005), Rainfall exclusion in an eastern Amazonian forest alters soil water movement and depth to water uptake, *Am. J. Bot.*, *92*, 443–455, doi:10.3732/ajb.92.3.443.

Schaller, M. F., and Y. Fan (2009), River basins as groundwater exporters and importers: Implications for water cycle and climate modeling, *J. Geophys. Res.*, *114*, D04103, doi:10.1029/2008JD010636.

Selhorst, D., S. A. Vieira, and I. F. Brown (2003), Agua e crescimento de uma floresta na Amazonia Sul-Ocidental, Acre, Brasil: Chuva afeta crescimento, mas nıvel do lencol freatico nao, poster report, Univ. Fed. do Acre, Rio Branco, Brazil. [ftp://lba.cptec.inpe.br/lba_archives/LC/LC-02/Posters/SelhorstDiogo_Poster_VI_CEB_02nov03.pdf.]

Singh, V. P. (2003), On the theories of hydraulic geometry, *Int. J. Sediment Res.*, *18*, 196–218.

Summerfield, M. A., and N. J. Hulton (1994), Natural controls of fluvial denudation rates in major world drainage basins, *J. Geophys. Res.*, *99*, 13,871–13,883, doi:10.1029/94JB00715.

Tanaka, T., M. Yasuhara, H. Sakai, and A. Marui (1988), The Hachioji experimental basin study–storm runoff processes and the mechanism of its generation, *J. Hydrol.*, *102*, 139–164, doi:10.1016/0022-1694(88)90095-9.

Tomasella, J., M. G. Hodnett, L. A. Cuartas, A. D. Nobre, M. J. Waterloo, and S. M. Oliveira (2008), The water balance of an Amazonian micro-catchment: The effect of interannual variability of rainfall on hydrological behavior, *Hydrol. Processes*, *22*, 2133–2147, doi:10.1002/hyp.6813.

Trigg, M. A., M. D. Wilson, P. D. Bates, M. S. Horritt, D. E. Alsdor, B. R. Forsbert, and M. C. Vega (2009), Amazon flood wave hydraulics, *J. Hydrol.*, *374*, 92–105, doi:10.1016/j.jhydrol.2009.06.004.

Troch, P. A., C. Paniconi, and E. E. van Loon (2003), Hillslope-storage Boussinesq model for subsurface flow and variable source areas along complex hillslopes: 1. Formulation and characteristic response, *Water Resour. Res.*, *39*(11), 1316, doi:10.1029/2002WR001728.

Vourlitis, G. L., J. D. Nogueira, F. D. Lobo, K. M. Sendall, S. R. de Paulo, C. A. A. Dias, O. B. Pinto Jr., and N. L. R. de Andrade (2008), Energy balance and canopy conductance of a tropical semi-deciduous forest of the southern Amazon Basin, *Water Resour. Res.*, *44*, W03412, doi:10.1029/2006WR005526.

Walko, R. L., et al. (2000), Coupled atmosphere-biophysics-hydrology models for environmental modeling, *J. Appl. Meteorol.*, *39*, 931–944, doi:10.1175/1520-0450(2000)039<0931:CABHMF>2.0.CO;2.

Walter, B. P., and M. Heimann (2000), A process-based, climate-sensitive model to derive methane emissions from natural wetlands: Application to five wetland sites, sensitivity to model parameters and climate, *Global Biogeochem. Cycles*, *14*(3), 745–765, doi:10.1029/1999GB001204.

Whalen, S. C. (2005), Biogeochemistry of methane exchange between natural wetlands and the atmosphere, *Environ. Eng. Sci.*, *22*, 73–94, doi:10.1089/ees.2005.22.73.

Whitmore, T. C. (1992), *An Introduction to Tropical Rainforests*, 226 pp., Clarendon Press, Oxford, U. K.

Wilson, M., P. Bates, D. Alsdorf, B. Forsberg, M. Horritt, J. Melack, F. Frappart, and J. Famiglietti (2007), Modeling large-scale inundation of Amazonian seasonally flooded wetlands, *Geophys. Res. Lett.*, *34*, L15404, doi:10.1029/2007GL030156.

Winter, T. C., J. W. Harvey, O. L. Franke, and W. A. Alley (1998), Ground water and surface water: A single resource, *U.S. Geol. Surv. Circ.*, *1139*, 79 pp.

Yamazaki, D., T. Oki, and S. Kanae (2009), Deriving a global river network map and its sub-grid topographic characteristics from a fine-resolution flow direction map, *Hydrol. Earth Syst. Sci.*, *13*, 2241–2251, doi:10.5194/hess-13-2241-2009.

Yamazaki, D., S. Kanae, H. Kim, and T. Oki (2011), A physically based description of floodplain inundation dynamics in a global river routing model, *Water Resour. Res.*, *47*, W04501, doi:10.1029/2010WR009726.

Yang, Z.-L., et al. (2011), The community Noah land surface model with multi-parameterization options (Noah-MP): 2. Evaluation over global river basins, *J. Geophys. Res.*, *116*, D12110, doi:10.1029/2010JD015140.

Yeh, P. J. F., and E. A. B. Eltahir (2005), Representation of water table dynamics in a landsurface scheme, Part I: Model development, *J. Clim.*, *18*, 1861–1880, doi:10.1175/JCLI3330.1.

York, J. P., M. Person, W. J. Gutowski, and T. C. Winter (2002), Putting aquifers into atmospheric simulation models: An example from Mill Creek Watershed, northeastern Kansas, *Adv. Water Resour.*, *25*(2), 221–238, doi:10.1016/S0309-1708(01)00021-5.

Yuan, X., and X.-Z. Liang (2011), Evaluation of a Conjunctive Surface-Subsurface Process Model (CSSP) over the Contiguous United States at Regional-Local Scales, *J. Hydrometeorol.*, *12*, 579–599, doi:10.1175/2010JHM1302.1.

Yuan, X., Z. H. Xie, J. Zheng, X. J. Tian, and Z. L. Yang (2008), Effects of water table dynamics on regional climate: A case study over east Asian monsoon area, *J. Geophys. Res.*, *113*, D21112, doi:10.1029/2008JD010180.

Zeng, X. B., and M. Decker (2009), Improving the numerical solution of soil moisture-based Richards equation for land models with a deep or shallow water table, *J. Hydrometeorol.*, *10*(1), 308–319, doi:10.1175/2008JHM1011.1.